AWARD NUMBER: W81XWH-16-1-0314

TITLE: Discovery and Characterization of PRCAT47: A Novel Prostate Lineage and Cancer-Specific Long Noncoding RNA

PRINCIPAL INVESTIGATOR: Rohit Mehra, M.D.

CONTRACTING ORGANIZATION: University of Michigan
Ann Arbor, MI 48109-5940

REPORT DATE: OCTOBER 2019

TYPE OF REPORT: Final

PREPARED FOR: U.S. Army Medical Research and Materiel Command
                Fort Detrick, Maryland 21702-5012

DISTRIBUTION STATEMENT: Approved for Public Release;
                Distribution Unlimited

The views, opinions and/or findings contained in this report are those of the author(s) and should not be construed as an official Department of the Army position, policy or decision unless so designated by other documentation.

REPORT DOCUMENTATION PAGE

Form Approved
OMB No. 0704-0188

Public reporting burden for this collection of information is estimated to average 1 hour per response, including the time for reviewing instructions, searching existing data sources, gathering and maintaining the data needed, and completing and reviewing this collection of information. Send comments regarding this burden estimate or any other aspect of this collection of information, including suggestions for reducing this burden to Department of Defense, Washington Headquarters Services, Directorate for Information Operations and Reports (0704-0188), 1215 Jefferson Davis Highway, Suite 1204, Arlington, VA 22202-4302. Respondents should be aware that notwithstanding any other provision of law, no person shall be subject to any penalty for failing to comply with a collection of information if it does not display a currently valid OMB control number. **PLEASE DO NOT RETURN YOUR FORM TO THE ABOVE ADDRESS.**

1. REPORT DATE	2. REPORT TYPE	3. DATES COVERED
OCTOBER 2019	Final	1JUL2016 - 30JUN2019

4. TITLE AND SUBTITLE

TITLE: Discovery and Characterization of PRCAT47: A Novel Prostate Lineage and Cancer-Specific Long Noncoding RNA

5a. CONTRACT NUMBER
W81XWH-16-1-0314

5b. GRANT NUMBER
PC150246

5c. PROGRAM ELEMENT NUMBER

6. AUTHOR(S)
Rohit Mehra, M.D.

E-Mail: mrohit@med.umich.edu

5d. PROJECT NUMBER

5e. TASK NUMBER

5f. WORK UNIT NUMBER

7. PERFORMING ORGANIZATION NAME(S) AND ADDRESS(ES)

Regents of the University of
Michigan
Ann Arbor, MI 48109-1340

8. PERFORMING ORGANIZATION REPORT NUMBER

9. SPONSORING / MONITORING AGENCY NAME(S) AND ADDRESS(ES)

U.S. Army Medical Research and Materiel Command
Fort Detrick, Maryland 21702-5012

10. SPONSOR/MONITOR'S ACRONYM(S)

11. SPONSOR/MONITOR'S REPORT NUMBER(S)

12. DISTRIBUTION / AVAILABILITY STATEMENT

Approved for Public Release; Distribution Unlimited

13. SUPPLEMENTARY NOTES

14. ABSTRACT
The overall goal of this project is to characterize the functioning mechanism, utility and therapeutic potential of the biomarker PRCAT47 in prostate cancer. During this second period, we investigated the regulatory effect of PRCAT47 on androgen receptor (AR)transcript stability. We also interrogated the role of PRCAT47 in regulating HuR/TIAR-targeted mRNAs. Utilizing a novel RNA in situ hybridization technology optimized within the first period which allows us to assess PRCAT47 expression in prostate tissues, we have not evaluated PRCAT47 expression in prostate cancer tissue microarrays by RNA-ISH and demonstrate an association with prostate cancer progression. Finally, we also assessed the therapeutic potential of PRCAT47 using cell line models and patient derived organoid cultures.

15. SUBJECT TERMS
Prostate cancer; long non-coding RNA; PRCAT47

16. SECURITY CLASSIFICATION OF:			17. LIMITATION OF ABSTRACT	18. NUMBER OF PAGES	19a. NAME OF RESPONSIBLE PERSON USAMRMC
a. REPORT	**b. ABSTRACT**	**c. THIS PAGE**	Unclassified	42	**19b. TELEPHONE NUMBER** *(include area code)*
Unclassified	Unclassified	Unclassified			

Standard Form 298 (Rev. 8-98)
Prescribed by ANSI Std. Z39.18

Table of Contents

1. Introduction

As the most commonly diagnosed type of cancer in American man, prostate cancer is the second leading cause of cancer-related death. Androgen receptor (AR) signaling plays a pivotal role in normal prostate development, as well as in cancer progression. Therefore, androgen deprivation therapy (ADT) has been developed as a front-line therapy for patients with localized prostate cancer. Despite the fact that ADT, combined with surgery and radiotherapy, is able to cure most of the patients with localized disease, metastasis occur when disease progress to castration-resistant state (CRPC). Treatment options are limited for these patients, due to the largely diverse pathological mechanisms. Some known drivers for CRPC include: AR amplifications, AR mutations, activation of androgen receptor (AR) signaling genes without AR, deregulated epigenetic modifiers, etc. During the last decade, study of long noncoding RNAs have uncovered their roles in the context of cancer, which includes diagnostic markers, prognostic markers, and modifiers of oncogenic or tumor suppressive pathways. Through dynamic interactions with proteins, RNA and chromatin, lncRNAs contribute to the six canonical hallmarks of cancer. It is thus worth investigating whether lncRNAs are involved in AR signaling and contribute to prostate cancer progressing to CRPC. In response to this question, our lab initiated a comprehensive profiling analysis to identify AR-regulated lncRNAs associated with prostate cancer progression. During this process, we identified lncRNA PRCAT47, which has prostate lineage-specific expression pattern, is directly regulated by AR, and is associated with prostate cancer progression. Functional study of this lncRNA indicates that it is important for cell proliferation and regulation of AR signaling. The aim of this study is to investigate the mechanism of PRCAT47 involvement in steroid-receptor signaling and evaluate it as a target for therapeutic intervention in prostate cancer.

2. Keywords

Prostate cancer, long non-coding RNA, PRCAT47

3. Accomplishments

Major goals of the project

The overall goal of this project was to characterize the role of long non-coding RNA PRCAT47 in regulating AR signaling pathway and in mediating prostate cancer progression. We hypothesized that PRCAT47 plays a critical role in regulating AR signaling and subsequently the development and progression of prostate cancer, and that it may be a promising therapeutic target for treating castration-resistant prostate cancer. Three specific aims were proposed to test this hypothesis:

Specific Aim 1: To elucidate the molecular mechanism of AR regulation by PRCAT47.
Specific Aim 2: To assess clinical utility of PRCAT47 as a prognostic or diagnostic biomarker.
Specific Aim 3: To interrogate the therapeutic potential of PRCAT47 *in vitro* and in *vivo*.

To achieve these goals, we have finished the research-specific tasks as planned in the proposal. Specifically, using RNA-immunoprecipitation, combined with RNA-Seq and single molecule imaging technologies, we delineated the roles of PRCAT47-binding proteins HuR and TIAR in regulating AR signaling. Using RNA *in-situ* hybridization, we evaluated the expression of PRCAT47 in prostate cancer tissue microarrays. Using cohorts with clinical outcomes, we investigated the clinical importance of PRCAT47 as biomarkers in predicting biochemical recurrence. Using antisense oligonucleotides, we interrogated the therapeutic potential of PRCAT47 in multiple models *in vitro* and *in vivo*.

Accomplishment under major goals

Specific Aim 1: To elucidate the molecular mechanism of AR regulation by PRCAT47 (Month 1-24).

Objectives and major activities:

We have previously identified PRCAT47 as a prostate-lineage specific long non-coding RNA with elevated expression in both primary and castration-resistance metastatic prostate cancer. Functional study of this lncRNA suggested that it contributes to cell proliferation and modulation of AR signaling. The objective of this aim is to thoroughly investigate the molecular mechanism of PRCAT47 using cell line models. This will also shed light on its role in regulating AR signaling. Many lncRNAs have been shown to carry out functions via binding interactions with proteins. To identify the protein binding partners of PRCAT47, we previously performed RNA pull-down assay followed by Mass Spectrometry analysis. Two proteins, HuR and TIAR, were identified as top proteins that bind with PRCAT47, both of which have been reported to bind with AU-rich elements and regulate stability of mRNAs. Specifically, HuR has been reported to regulate AR mRNA through its 3'UTR.

We hypothesized that PRCAT47 regulates transcriptome through its two binding partners, HuR and TIAR. This aim specifically focused on investigating the role of HuR and TIAR in PRCAT47-mediated regulation of AR signaling (Subtask 1) and examining the role of PRCAT47 and its interacting proteins in global RNA regulation (Subtasks 2 and 3).

Key outcomes and conclusions:

Post-transcriptional regulation of AR signaling by PRCAT47

As the first step of understanding the mechanisms of PRCAT47 regulation on AR signaling, we studied the effect of PRCAT47 loss on AR mRNA and protein stability (**Figure 1**). Compared to GAPDH mRNA, which is not affected by PRCAT47 depletion, we observed a decreased AR mRNA stability after PRCAT47 knockdown (**Figure 1a**). Diminished levels of AR protein could also be observed upon PRCAT47 loss (**Figure 1b**). Furthermore, we utilized a BrU/BrUChase labeling assay followed by RNA-Seq or qPCR to measure RNA synthesis rate and RNA stability. We observed that the AR mRNA synthesis rate (BrU RNA) is not affected by PRCAT47 loss, while the stability of AR mRNA (BrUChase RNA) decreased significantly (**Figure 1d**). More interestingly, the sequencing track at AR locus indicated that the decreased AR mRNA stability is preferentially observed at the 3'UTR region of AR. These results demonstrated that PRCAT47 is likely to regulate AR through post-transcriptional processes.
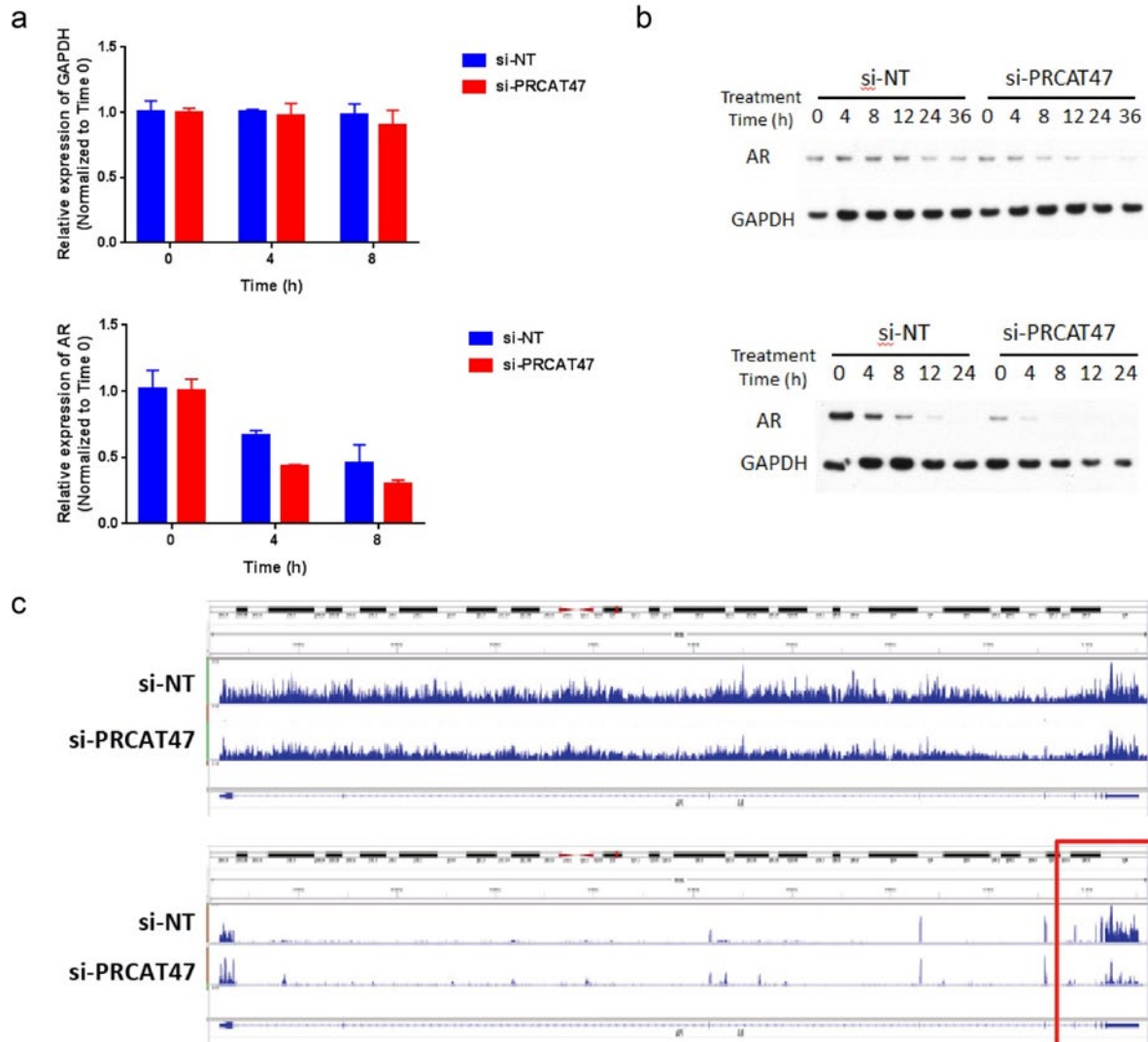
d
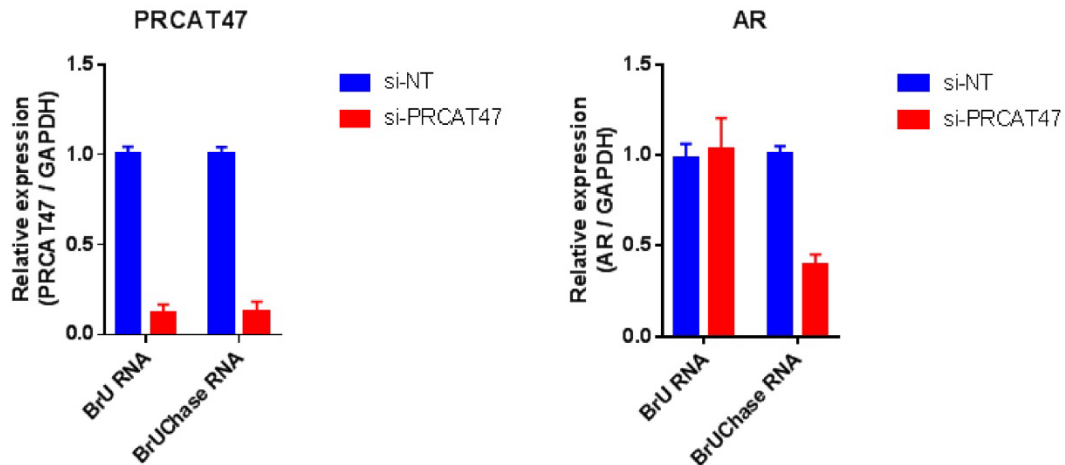
Figure1: Post-transcriptional regulation of AR by PRCAT47
(a) Relative amount of GAPDH (Up) and AR (Bottom) mRNA change in MDA-PCa-2b cells following Actinomycin D treatment for 0, 4 and 8 hours, under PRCAT47 knockdown or control condition.
(b) Western blot analysis of AR and GAPDH protein in LNCaP cells (Up) or MDA-Pca-2b cells (Bottom) following cyclohexamide treatment for indicated time periods, under PRCAT47 knockdown or control condition.
(c) BrU-Seq (Top) and BrUChase-Seq tracks (Bottom) at AR genomic locus from MDA-PCa-2b cells.
(d) BrU-PCR and BrUChase-PCR results for PRCAT47 transcript (Left) and for AR transcript (Right) in MDA-PCa-2b cells, following treatment of siRNA targeting PRCAT47.

Involvement of HuR and TIAR in AR signaling regulation

To investigate whether PRCAT47-interacting proteins are involved in PRCAT47 regulation on its target genes (including AR), we next assessed the concordance of genes whose expression is most altered upon knockdown of PRCAT47, HuR, and TIAR, using RNA-Seq analysis (**Figure 2a and Figure 2b**). We discovered a total of 7125 and 5258 genes that are significantly regulated by HuR or TIAR, respectively. Furthermore, we derived AR signaling gene signature from DHT-stimulated MDA-PCa-2b cells (**Figure 2c**). When overlapping these data with RNA-Seq results gained following PRCAT47 knockdown, we found a significant overlap between PRCAT47 target genes and HuR-regulated genes (**Figure 3a Top**). Meanwhile, we observed a modest overlap between PRCAT47 target genes and TIAR-regulated genes (**Figure 3a Bottom**). These observations indicate that PRCAT47 is likely to affect target genes through its protein interactors HuR and TIAR. Moreover, we performed Gene Set Enrichment Analysis and observed the enrichment of AR signaling pathway in HuR- and TIAR-regulated transcriptome.

These results suggest that PRCAT47 is likely to convey its functions through protein interactors HuR and TIAR. Both HuR and TIAR are involved in AR signaling modulation.

Figure 2: Gene expression profiling following HuR or TIAR knockdown or DHT stimulation
(a) Gene expression profile following HuR knockdown in MDA-PCa-2b cells and LNCaP cells. The most significant HuR regulated genes were illustrated in the heatmap.
(b) Gene expression profile following TIAR knockdown in MDA-PCa-2b cells and LNCaP cells. The most significant TIAR regulated genes were illustrated in the heatmap.
(c) Reproducibility of expression profiling following 10nM DHT treatment in MDA-PCa-2b cells. The most significant AR targets were used to derive a gene signature of AR response.

Figure 3: Overlap between RNA-Seq-derived gene signatures
(a) Up: Venn Diagram illustrating overlap between genes significantly regulated by HuR and PRCAT47. Bottom: Venn Diagram illustrating overlap between genes significantly regulated by TIAR and PRCAT47.
(b) Enrichment of AR signaling gene set in HuR regulated transcriptome (NES=normalized enrichment score)
(c) Enrichment of AR signaling gene set in TIAR regulated transcriptome (NES=normalized enrichment score)

Since HuR and TIAR are AU-rich element binding proteins that regulate mRNA stability, we next sought to delineate the mRNAs that directly bind with HuR and TIAR, and interrogated whether the binding is affected by PRCAT47. Specifically, we asked whether HuR/TIAR directly interacts with AR mRNA and whether the interaction is mediated by PRCAT47. We carried out RNA-immunoprecipitation (RIP) using HuR or TIAR antibodies and profiled the RNAs pulled down by RNA-Seq (**Figure 4a-b**). A common set of RNA species were identified as HuR- or TIAR-bound RNAs across two prostate cancer cell lines. We noticed that a large number of RNAs interact with HuR or TIAR protein. This can be explained by the ubiquitous presence of the two proteins in RNA processing and mRNA stabilization processes. We reasoned that not all physical interactions between RNA and protein would result in regulation on RNA stability. Therefore, to identify the RNA species that directly bind with HuR (or TIAR) and modulated by HuR (or TIAR), we intercepted RIP-Seq data with the aforementioned HuR/TIAR-regulated RNAs identified from RNA-Seq. These transcripts were defined as direct HuR (or TIAR) targets (**Figure 4c-d**).
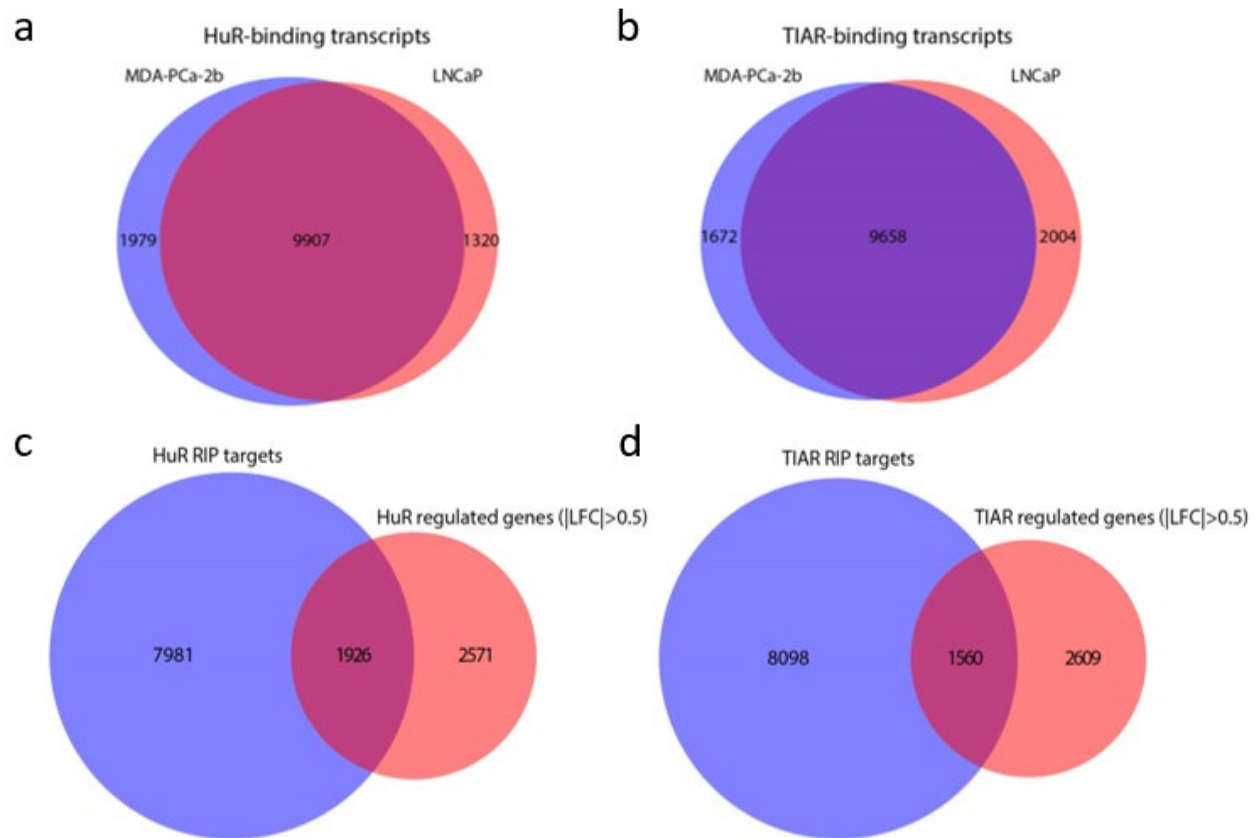
Figure 4: Direct mRNA targets of HuR and TIAR

(a) Venn Diagrams illustrating number of transcripts bound by HuR in MDA-PCa-2b cells and LNCaP cells.

(b) Venn Diagrams illustrating number of transcripts bound by TIAR in MDA-PCa-2b cells and LNCaP cells.

(c) Venn Diagrams indicating overlap between transcripts bound by HuR, and transcripts regulated by HuR.

(d) Venn Diagrams indicating overlap between transcripts bound by TIAR, and transcripts regulated by TIAR.

Moreover, we discovered that around 25% of all PRCAT47 regulated transcripts are direct HuR targets or TIAR targets (**Figure 5a-b**). Loss of PRCAT47 and loss of HuR induces similar expression changes in this set of genes (**Figure 5c**). Interestingly, AR is within this gene set. This observation indicates that PRCAT47 is likely to be involved in HuR-mediated maintenance of mRNA stability, and that the post-transcriptional regulation of PRCAT47 on AR signaling might be achieved via HuR.
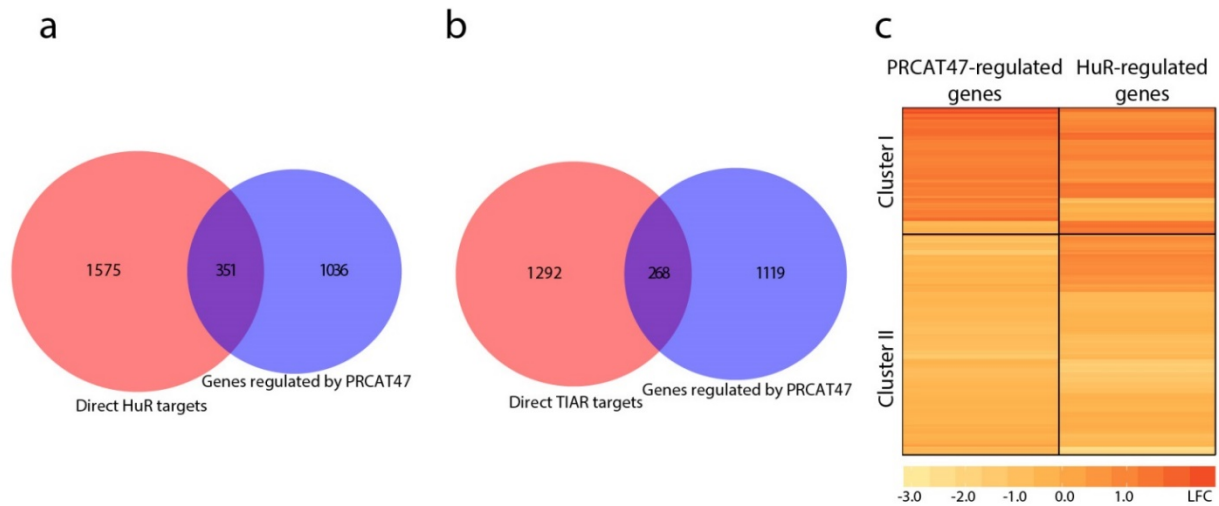
Figure 5: Overlap between PRCAT47-regulated genes and direct HuR/TIAR targets.
(a) Venn Diagram indicating the overlapped gene number between direct HuR targets and PRCAT47-responsive targets.
(b) Venn Diagram indicating the overlapped gene number between direct TIAR targets and PRCAT47-responsive targets.
(c) A heatmap representing the degree of gene expression change (indicated by LFC) of PRCAT47-responsive HuR targets following loss of PRCAT47 or HuR.

To further validate the interplay between HuR and AR mRNA, and test whether this interaction is modulated by PRCAT47, we performed RNA-immunoprecipitation using HuR-specific antibody, and detected the bound mRNAs using qPCR analysis. In accord with reports in literatures, we observed interactions between HuR and AR mRNA, HuR and Actin mRNA (positive control) (**Figure 6**). To investigate the role of PRCAT47 in this process, we repeated the RIP-qPCR analysis in cells transfected with siRNA targeting PRCAT47. As a control, relative binding between HuR and Actin mRNA did not alter significantly (**Figure 6, Right**). In contrast, upon PRACT47 loss, relative binding between HuR and AR mRNA decreased significantly (**Figure 6, Left**).

Together, these results suggest that PRCAT47-induced transcriptome change is at least partially achieved through HuR and TIAR. PRCAT47 affects binding between HuR and AR mRNA, and the post-transcriptional regulation of AR mRNA by PRCAT47 is likely to be mediated by HuR protein.
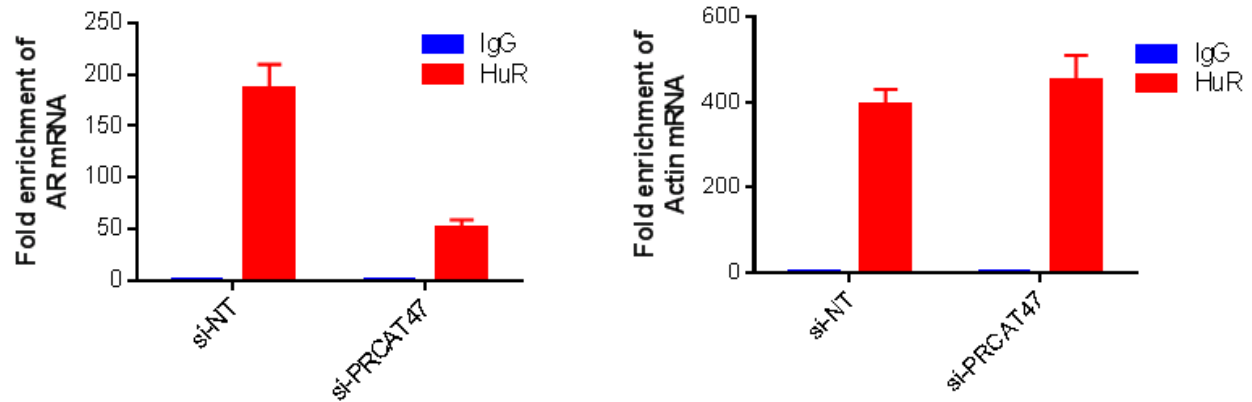
Figure 6: RNA immunoprecipitation followed by qPCR assays using HuR antibody
Fold enrichment of AR mRNA (Left) and Actin mRNA (Right) measured by qPCR analysis following RNA immunoprecipitation by HuR antibody or IgG. RIP experiment was performed in MDA-PCa-2b cells, following transfection of non-targeting siRNA or siRNA targeting PRCAT47.

Localization of PRCAT47 to stress granule

In our pilot experiments, we found that several PRCAT47-interacting proteins (TIAR, HuR, G3BP1, YB1, etc) are components associated with stress granule formation. We thus hypothesized that PRCAT47 may localize to stress granule and regulate stress granule formation. To test this hypothesis, we performed RNA fluorescence *in situ* hybridization (RNA-FISH) experiments, and labeled stress granules using antibodies for stress-granule associated proteins. We observed formation of stress granule following cell stress (**Figure 7a**).

Compared to GAPDH mRNA, a significantly larger percent of PRCAT47 transcript localized to stress granule (**Figure 7a-b**). The result suggests that PRCAT47 might be involved in stress granule formation. In fact, stress granules have reported implications in tumor progression by inhibiting apoptosis. Given the pro-apoptosis phenotypes observed upon PRCAT47 knockdown, it is possible that PRCAT47 contributes to stress granule formation, thus favoring tumor progression.
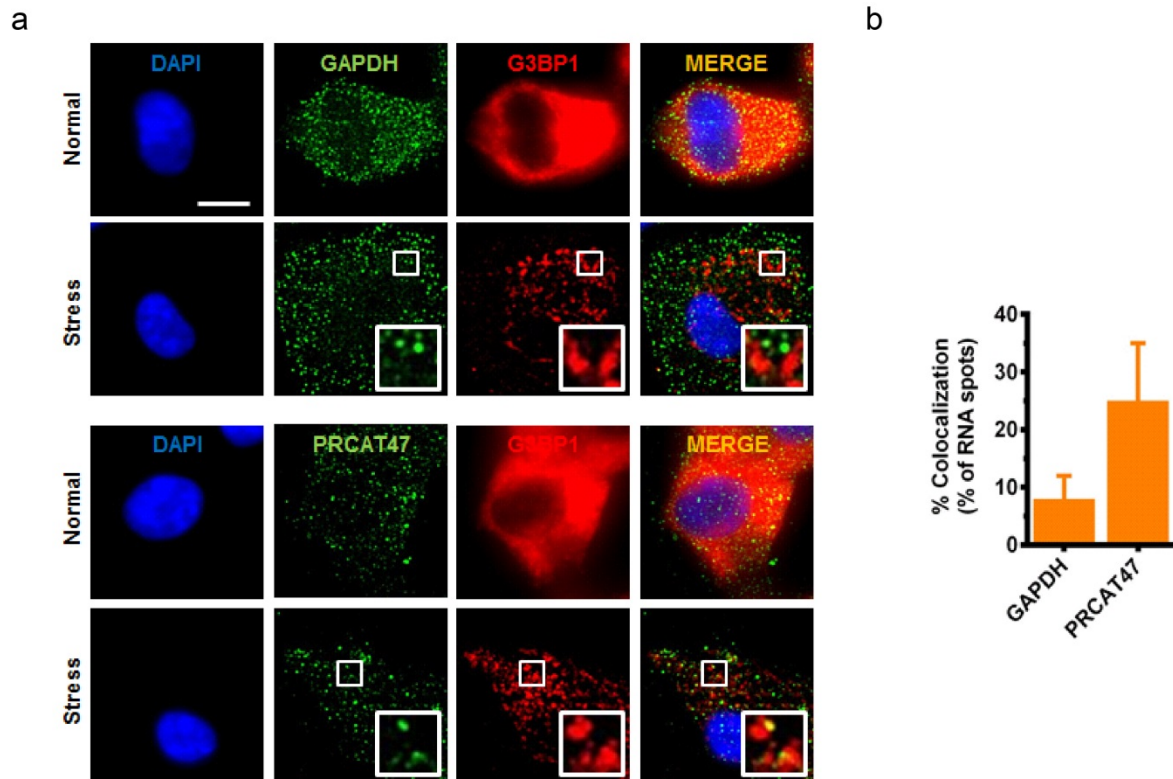
Figure 7: PRCAT47 localizes to stress granule under stress condition
(a) Representative pseudocolored images of cells stained for the appropriate transcripts, proteins, or DAPI, under normal or stressed conditions.
(b) Quantified co-localization of indicated RNAs and stress granule

Specific Aim 2: To assess clinical utility of PRCAT47 as a prognostic or diagnostic biomarker (Month 6-36)

Objectives and major activities:

Diagnostic assays for clinical prostate cancer detection has been limited to serum PSA and PCA3 test. However, these assays cannot effectively distinguish indolent prostate cancer from an aggressive disease. Additional diagnostic and prognostic markers are needed to overcome this challenge. Our preliminary data demonstrated that PRACT47 expression is limited to prostate cancer lineage. Abundance of this transcript is higher in cancer compared to normal tissues. In this aim, we assess the potential of PRCAT47 as a prognostic or diagnostic biomarker. Specifically, we explored the expression of PRCAT47 in prostate cancer outcome arrays (Subtask 1 and 2). In addition, we assessed the expression of PRCAT47 in prostate cancer tissue microarrays (TMAs) by RNA-*in situ* hybridization (ISH) (Subtask 3).

Key outcomes and conclusions:

PRCAT47 as a biomarker for predicting biochemical recurrence

Using Affymetrix Human Exon microarray data generated from cohorts with clinical outcome information, we evaluated the clinical importance of PRCAT47 as a prognosis marker. In the cohort from Mayo clinic, PRCAT47 was able to predict freedom from biochemical recurrence. Lower PRCAT47 expression suggests a lower opportunity of developing biomedical recurrence.
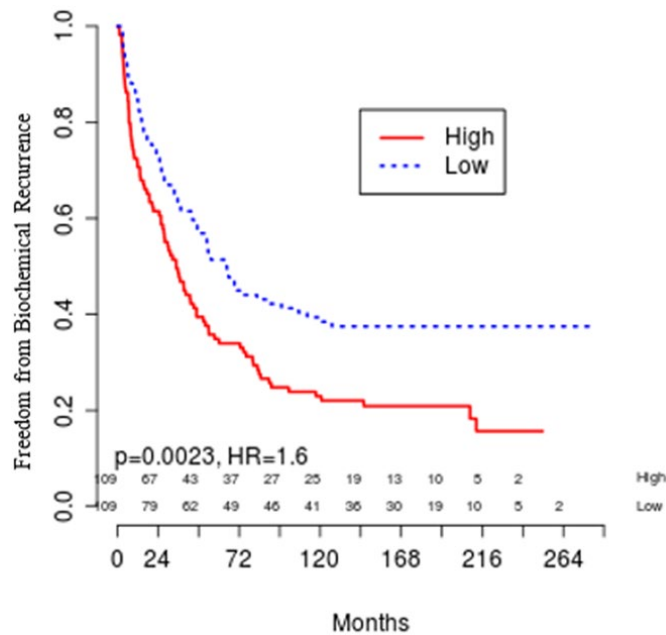
Figure 8: Kaplan Mayer analysis of PRCAT47 expression to predict for biochemical recurrence.

Evaluation of PRCAT47 in prostate cancer tissue microarrays by ISH

We have developed probes for PRCAT47, as well as an *in situ* hybridization (ISH) assay to detect transcript expression levels in formalin-fixed paraffin-embedded (FFPE) tissues represented on tissue microarrays (TMAs). Briefly, FFPE sections were baked at 60°C for one hour. Tissues were deparaffinized by immersing in xylene twice for five minutes each with periodic agitation. The slides were immersed in 100% ethanol twice for one minute each with periodic agitation and then air-dried for five minutes. After a series of pretreatment steps, the cells were permeabilized using Protease Plus to allow probes access to the RNA target. Hybridization of the probes to the RNA targets was performed by incubation in the HybEZ™ Oven for two hours at 40°C. After two washes, the slides were processed for standard signal amplification steps. Chromogenic detection was performed using DAB followed by counterstaining with 50% Gill's Hematoxylin I.

Slides were examined for PRCAT47 ISH signals in morphologically intact cells. PRCAT47 ISH signal was identified as brown, punctate dots, and expression level was scored as follows: 0 = no staining or less than 1 dot per 10 cells, 1 = 1 to 3 dots per cell, 2 = 4 to 9 dots per cell (few or no dot clusters), 3 = 10 to 15 dots per cell (less than 10% in dot clusters), and 4 = greater than 15 dots per cell (more than 10% in dot clusters). A cumulative ISH product score was calculated for each evaluable tissue core as the sum of the individual products of the expression level (0 to 4) and percentage of cells (0 to 100) (i.e., [A%× 0] + [B%× 1] + [C%× 2] + [D% × 3] + [E% × 4]; total range = 0 to 400). For each tissue sample, the ISH product score was averaged across evaluable TMA tissue cores.

We have performed RNA-ISH expression of PRCAT47 in a spectrum of tissues representing benign prostatic tissue, clinically localized prostate cancer (with associated long-term clinical follow-up information) and metastatic hormone refractory prostate cancer (from a unique cohort of "rapid autopsy" patients at University of Michigan). Representative PRCAT47 staining is shown for benign prostate, localized, and metastatic prostate cancer tissue (**Figure 9**). Bar plot represents mean PRCAT47 expression scores across benign, localized, and metastatic tissues, with vertical bars indicating bootstrapped 95% CI of the means. Significance was calculated by a Kruskal-Wallis rank sum test.

The PRCAT47 expression level is significantly higher in localized cancer and metastatic disease, compared with benign prostate. This result is in accord with our previous observation obtained from analyzing RNA-seq data. However, PRCAT47 expression is not significantly higher in metastatic disease than in primary prostate cancer. This does not contradict the observation that PRCAT47 is one of the most differentially expressed transcripts identified from both "PCa vs. Normal analysis" and "Mets vs. Normal analysis".
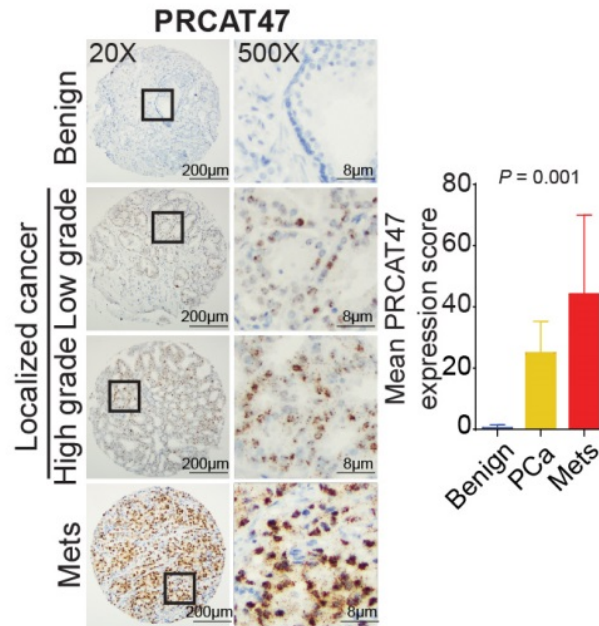
Figure 9: Evaluation of PRCAT47 expression across different grades of prostate cancer samples.
Left, representative PRCAT47 ISH images of benign prostate, localized prostate cancer, and metastasis prostate cancer samples. Right, quantified PRCAT47 expression scores in prostate cancer sample groups of various grades.

Clinical relevance of PRCAT47

We further tested whether PRCAT47 expression is associated with Gleason score in the primary prostate cancer tissues. In contrast to established prognostic markers in prostate cancer (such as AURKA), PRCAT47 did not show a clear association with Gleason score (**Figure 10a**). PRCAT47 is therefore not a biomarker to stratify cancers with varied aggressiveness, although it will be important to reassess this once outcomes data becomes available for the SU2C/PCF mCRPC cohort.

We next asked whether samples with high PRCAT47 levels are characterized by a more aggressive transcriptional phenotype. We compared the top- and bottom-quartiles of samples based on PRCAT47 expression, and as expected found that the top-samples were characterized by elevated expression of "Androgen Receptor Signaling Targets" genes (**Figure 10b**) and an expression profile consistent with luminal epithelial prostate cancer (**Figure 10c**), which was also reflected in the down-regulation of genes associated with the epithelial-to-mesenchymal transition (**Figure 10d**).

While oncogenic AR-signaling is the primary driver of PCa, it also associated with the terminal differentiation of prostate cells. At the stage of castration resistance, tumors that become AR-independent or neuroendocrine are often associated with poorer outcomes. PRCAT47 tumors remain AR-dependent and may benefit at least partially from next-generation anti-androgens, which may improve their outcomes. Overall, the negative oncogenic activity of PRCAT47 may be counterbalanced in terms of outcomes by the high AR-dependence of PRCAT47-high tumors.

Figure 10: Clinical relevance of PRCAT47
(a) PRCAT47 expression levels are not associated with Gleason score. AURKA expression levels are significantly associated with Gleason score.
(b) Cancer hallmark signature analysis between PRCAT47 high (top-quartile) and PRCAT47 low (bottom-quartile) mCRPC samples. Z-score represents the effect-size and direction for the relative signature enrichment.
(c) Curated pathway signature analysis between PRCAT47 high (top-quartile) and PRCAT47 low (bottom-quartile) mCRPC samples. Z-score represents the effect-size and direction for the relative signature enrichment.
(d) Signatures associated with prostate cancer and luminal differentiation were selected from the MSigDB and contrasted between PRCAT47 high (top-quartile) and PRCAT47 low (bottom-

quartile) mCRPC samples. Z-score represents the effect-size and direction for the relative signature enrichment.

Specific Aim 3: To interrogate the therapeutic potential of PRCAT47 using clinical grade antisense oligonucleotides (Month 6-36)

Objectives and major activities:

In our preliminary experiments, we demonstrated that knocking down PRCAT47 by small interfering RNAs significantly inhibits cell proliferation and induces apoptosis. Because PRCAT47 is required for cell growth and is abundantly expressed in localized and metastatic prostate cancers, we hypothesized that PRCAT47 could be developed into a therapeutic target. In this aim, we utilized antisense oligonucleotides (ASOs) to evaluate therapeutic potential of PRCAT47 *in vitro* and *in vivo*. Specifically, we characterized the on-target knockdown efficacy, gene expression changes, and phenotypic effects induced by PRCAT47 ASOs *in vitro* (Subaim a). Moreover, we interrogated the therapeutic potential of PRCAT47 using a series of cell-line derived or patient-derived xenografts (Subaim b).

Key outcomes and conclusions:

Interrogating therapeutic potential of PRCAT47 *in vitro*

In collaboration with the *Ionis Pharmaceuticals*, we have developed antisense oligonucleotides (ASOs) targeting different regions on the PRCAT47 transcript. All of these ASOs demonstrated high on-target knockdown efficacy (**Figure 11a**). To compare the transcriptome changes induced by ASO- or siRNA-mediated knockdown, we performed correlation analysis following PRCAT47 loss induced by the two different methods in replicated microarray experiments in MDA-PCa-2b cells. The result confirmed a significant overlap between differentially expressed genes following PRCAT47 ASO or siRNA treatment (**Figure 11b**). Furthermore, similar to the effects generated by siRNA, we observed decreased expression of AR signaling genes (**Figure 11c**), as well as delayed cell proliferation in cells transfected with PRCAT47 ASOs (**Figure 11d**).
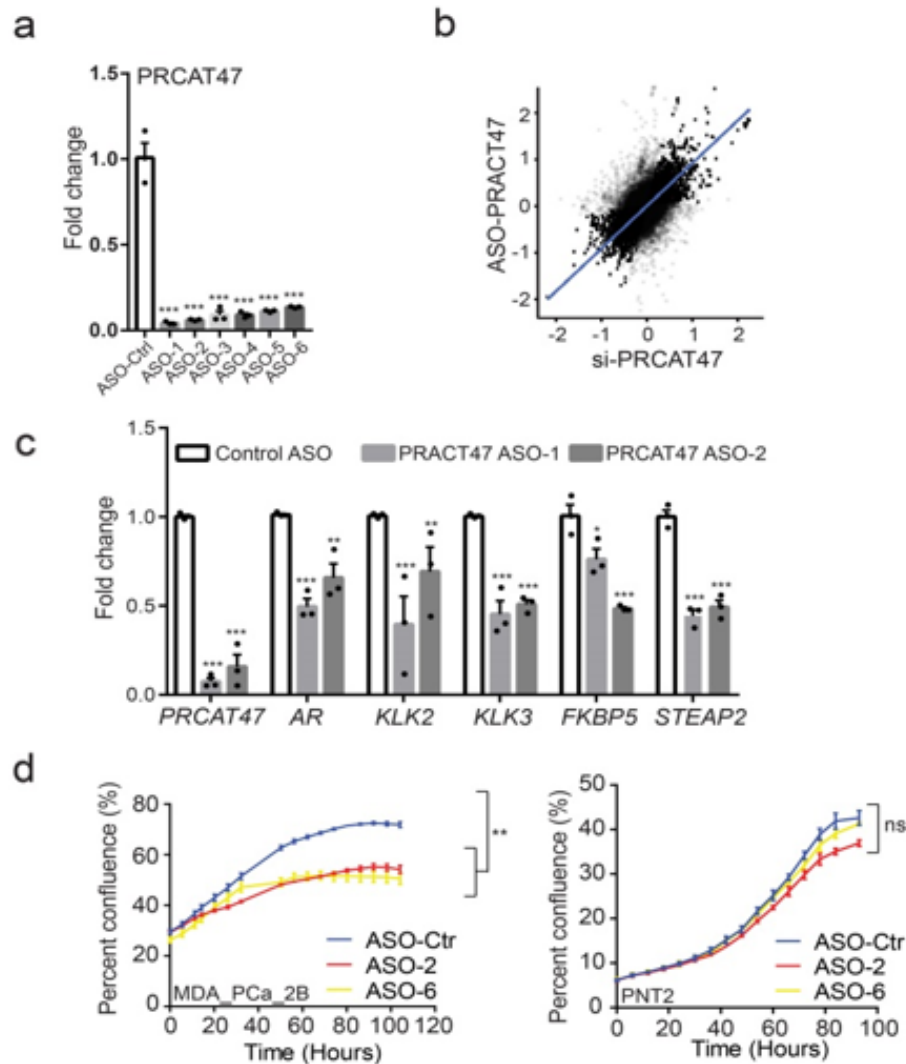
Figure 11: Characterization of ASOs targeting PRCAT47 in vivo
(a) MDA-PCa-2b cells were transfected with six independent ASOs targeting PRCAT47.
Knockdown efficacy was evaluated by qPCR analysis. Mean ± s.e.m are shown, n = 3.
(b) Correlation analysis of siRNA-mediated knockdown and ASO-mediated knockdown of
PRCAT47 in replicated microarray experiments in MDA-PCa-2b cells. Each dot represents a
gene. Combined significance level is indicated in shades of gray (black – most significant).
(c) qRT–PCR analysis of *PRCAT47*, *AR*, and *AR* target gens (*KLK2*, *KLK3*, *FKBP5*, and
STEAP2) in MDA-PCa-2b cells transfected with ASOs against *PRCAT47*. Data were normalized
to GAPDH and the levels in control ASO-treated cells were set to 1. Mean ± s.e.m. are shown, n
= 3
(d) Transfection of ASOs targeting PRCAT47 in AR-positive MDA-PCa-2b cells inhibits cell
proliferation. AR-negative prostate cell line PNT2 serves as negative control. Cell proliferation
was recorded using IncuCyte live cell monitoring system.

To be successfully used *in vivo*, one prerequisite is the ability of ASOs to be freely taken up by cells. We thus evaluated the knockdown efficiency of ASOs by prostate cancer cells without any lipid-based reagents. An average of ~60% knockdown was achieved across 6 ASOs tested (**Figure 12a**). Another prerequisite for ASOs to be applied *in vivo* is low toxicity. Aided *by Ionis Pharmaceuticals*, we were able to exclude the ASOs that demonstrated relatively high toxicity in mice models, and selected two clinical grade ASOs out of the six candidates. Delivery of these ASOs by cell free-uptake significantly inhibits cell growth in PRCAT47-positive cell line models (**Figure 12b**).
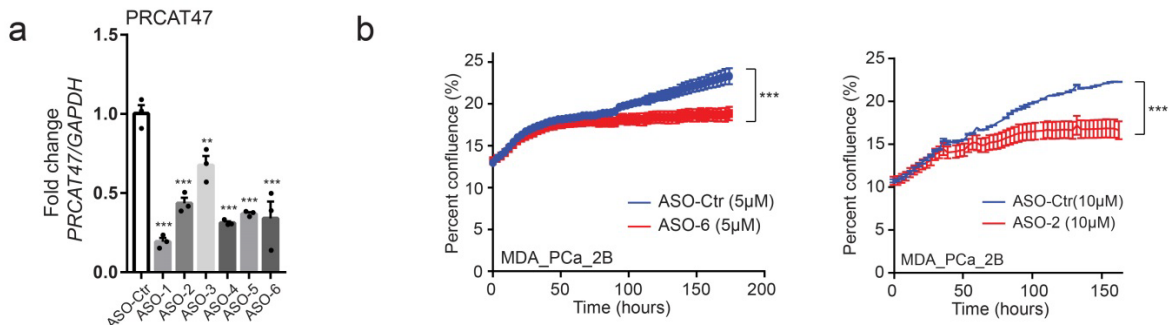
Figure 12: Free-uptake efficacy of ASOs targeting PRCAT47
(a) Free-uptake efficacy of PRCAT47 ASOs was examined in MDA-PCa-2B cells 72 hours after adding ASO to the medium (10 µM). PRCAT47 expression was evaluated by qPCR analysis. Mean ± s.e.m are shown, n = 3.
(b) Treatment of ASOs targeting PRCAT47 results in retarded growth of MDA-PCa-2b cells *in vitro*. PRCAT47-negative prostate cell line PNT2 serves as negative control. Cell proliferation was recorded using IncuCyte live cell monitoring system.

Interrogating therapeutic potential of PRCAT47 *in vivo*

Following the *in vitro* characterization of PRCAT47 ASOs, we further assessed the therapeutic potential of PRCAT47 *in vivo* using patient-derived or cell line-derived xenografts. To identify proper models to use, we first queried the PRCAT47 expression level in RNA-sequencing data generated from a panel of patient derived xenografts (PDXs) (**Figure 13a**). Of all PDX models that are available in lab, MDA-146-12 model has the highest PRCAT47 expression (**Figure 13a-b**). The efficacy of ASO was tested in this patient-derived xenograft. Six to eight week old male athymic nude mice were inoculated subcutaneously with suspended cells from MDA-146-12 patient derived xenograft in the posterior dorsal flank region (5 million cells/site, two sites / animal). When the mean tumor volume reached approximately 150 mm^3, mice were randomized into two groups, respectively treated with PRCAT47-specific or control ASO. ASOs, dosed 50 mg/kg, were subcutaneously injected between the scapulae once daily for a week (five days on/two days off). Mice were then sacrificed and the primary tumors were excised for RNA

extraction and ASO free-uptake evaluation (by qPCR analysis). Although compared to cell line models, expression level of PRCAT47 is not very high in MDA-146-12, we still observed a significant on-target effect of ASOs *in vivo* (**Figure 13c**).

Next, we assessed the *in vivo* efficacy of PRCAT47 ASOs using MDA-PCa-2b cell line derived xenografts. 6- to 8-week-old male athymic nude mice were inoculated subcutaneously with MDA-PCa-2b cells in the dorsal flank region. When the mean tumor volume reached approximately 150 mm^3, mice were randomized into two groups and treated with PRCAT47-specific or control ASO, dosed at 50 mg per kg body weight. ASOs were subcutaneously injected between the scapulae once daily for three periods of 5 days on/2 days off. Tumor size was measured twice per week using a digital caliper by a researcher blinded to the study design. When the average tumor size in the control group reached 1,500 mm^3, mice were euthanized and the primary tumors were excised and analyzed for gene expression changes.

Treatment of mice bearing MDA-PCa-2b xenografts with PRCAT47-targeting ASOs led to significant decreases in tumor growth compared to control ASO (**Figure 13d**). As expected, diminished expression of PRCAT47, as well as PRCAT47 target genes (like NKX3.1) were observed in these xenografts (**Figure 13e**). Taken together, these data suggest that PRCAT47 plays a critical role in the proliferation of AR-dependent prostate cancer and can be effectively exploited as a therapeutic target.
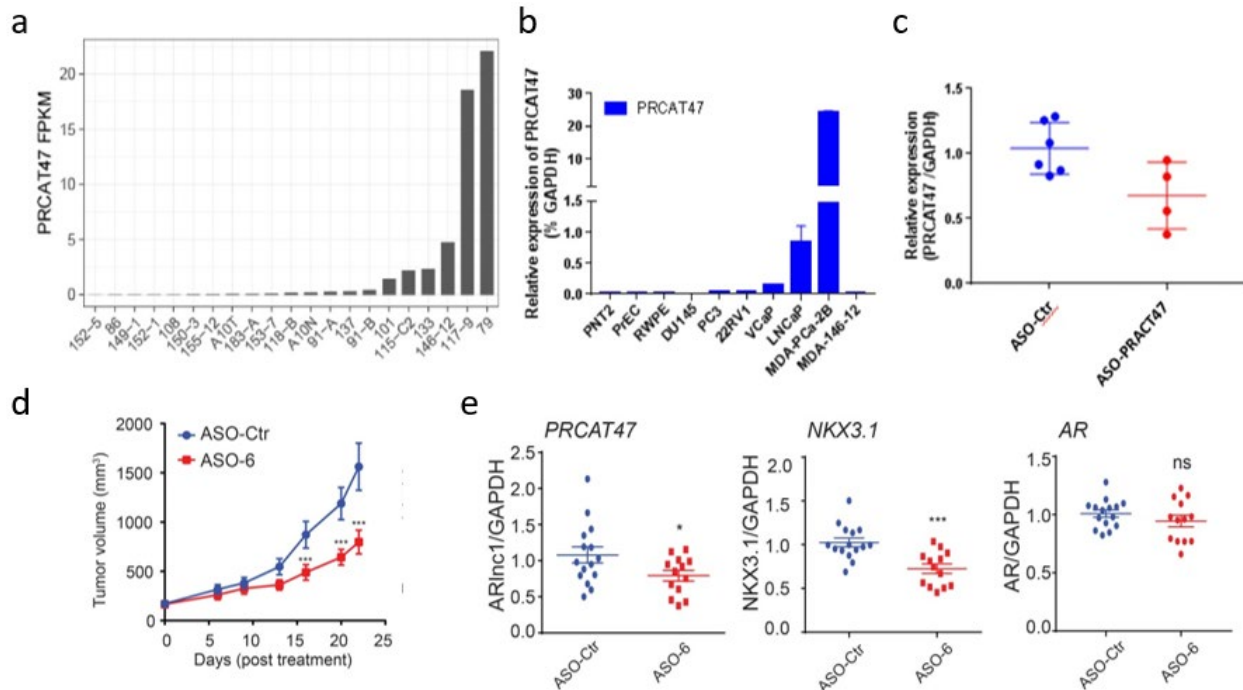
Figure 13: Therapeutic potential of PRCAT47

(a) Expression of PRCAT47 in a panel of patient-derived xenografts of prostate cancer (measured by FPKM value from RNA-Seq analysis)

(b) Expression of PRCAT47 across a panel of prostate cancer cells, and patient-derived xenograft MDA-146-12, measured by qPCR analysis.

(c) Relative expression of PRCAT47 in MDA-146-12 patient derived xenografts treated for control ASOs or ASO targeting PRCAT47, measured by qPCR analysis.

(d) Effect of ASO treatment on the growth of MDA-PCa-2b xenografts in male athymic nude mice, with control ASO or PRCAT47 ASO treatment subcutaneously at 50 mg per kg body weight, five times per week for 3 weeks. The graph shows changes in tumor volume, which was measured by caliper biweekly.

 (e) qRT–PCR analysis of PRCAT47, NKX3.1, and AR in MDA-PCa-2b xenografts treated with control ASO or ASO targeting PRCAT47. Data were normalized to a housekeeping gene (GAPDH), and the average expression level in the control ASO group was set to 1. Mean ± s.e.m. values are shown. *P = 0.0483, ***P = 0.0004, ns: not significant; compared to control group by two-tailed Student's t test.

4. Impact

What was the impact on the development of the principle discipline(s) of the project?

In the past decades, advances in next-generation sequencing enabled the discovery of long non-coding transcripts, a new category of molecules that function in a spatiotemporal manner in normal tissue development and oncogenesis process. In cancer context, though lncRNA expression landscape has been comprehensively profiled by several studies, their clinical utilities, functioning mechanisms, and therapeutic potential remain largely unknown. To start to fulfill this knowledge gap, our group initiated a systematic study to identify lncRNAs regulated by AR signaling and contribute to prostate cancer progression. Through this analysis, we discovered a lncRNA, PRCAT47 (a.k.a. ARLNC1), which exhibited a strong transcriptional induction by AR, is expressed in a prostate tissue-specific manner, and has elevated expression in localized and metastatic prostate cancer. We also observed that loss of this lncRNA inhibits cancer cell growth, and affects AR signaling.

In the course of this project, several key research milestones were accomplished, regarding PRCAT47 functional mechanisms, and its potential role as therapeutic target. (1) We characterized a novel node on AR signaling regulation network. PRCAT47 modulates AR post-transcriptionally, and lncRNA-interacting proteins are likely to be involved in this regulation process. (2) PRCAT47 is critical for prostate cancer progression. It could be inhibited using antisense oligonucleotides in

several models *in vitro* and *in vivo*, suggesting the possibility of targeting oncogenic lncRNA therapeutically in cancer.

What was the impact on other disciplines?

Nothing to report

What was the impact on technology transfer?

Nothing to report

What was the impact on society beyond science and technology?

Nothing to report

5. Changes/Problems

Nothing to report

6. Products

Journal publications, conference papers, and presentations

Yajia Zhang*, Sethuramasundaram Pitchiaya*, Marcin Cieślik*, Yashar S. Niknafs, Jean C-Y.Tien, Yasuyuki Hosono, Matthew K. Iyer, Sahr Yazdani, Shruthi Subramanyiam, Sudhanshu K. Shukla, Xia Jiang, Lisha Wang, Tzu-Ying Liu, Michael Uhl, Alexander Gawronski, Yuanyuan Qiao, Lanbo Xiao, Saravana M. Dhanasekaran, Kristin M. Juckette, Lakshmi P. Kunju, Xuhong Cao, Utsav Patel, Mona Batish, Girish C. Shukla, Michelle T. Paulsen, Mats Ljungman, Hui Jiang, Rohit Mehra, Rolf Backofen, Cenk S. Sahinalp, Sue Freier, Andy Watt, Shuling Guo, John T. Wei, Felix Y. Feng, Rohit Malik[#], Arul M. Chinnaiyan[#]. **Analysis of the androgen receptor-regulated lncRNA landscape identifies a role for ARLNC1 in prostate cancer progression.** *Nature Genetics*, May 28, 2018, doi: 10.1038/s41588-018 -0120-1 (ARLNC1 is another name for PRCAT47)

7. Participants & Other Collaborating Organizations

Name:	Rohit Mehra
Project Role:	Principal Investigator
Researcher Identifier (e.g. ORCID ID):	0000-0002-6955-8884
Nearest person month worked:	3
Contribution to Project:	Dr. Mehra has supervised proposed research and study personnel, drafted experiments, constructed tissue microarrays (TMAs) from various clinical cohorts of patients with localized and metastatic prostate cancer, performed and optimized RNA in situ Hybridization (RNA-ISH).
Funding Support:	DOD

Name:	Rohit Malik
Project Role:	
Nearest person month worked:	1
Contribution to Project:	Dr. Malik assisted with the functional characterization of the lncRNAs.

Name:	Pankaj Vats
Project Role:	Analyst

Nearest person month worked:	4
Contribution to Project:	Mr. Vats helped in the analysis of the high throughout data including RIP-Seq and ChIRP-seq.

Name:	Xia Jiang
Project Role:	Technician
Nearest person month worked:	3
Contribution to Project:	Ms. Zhang performed cell culture, various functional studies as well as molecular biology experiments.

8. Special Reporting Requirements

Nothing to report

9. Appendices

(1) Journal article:
Yajia Zhang*, Sethuramasundaram Pitchiaya*, Marcin Cieślik*, Yashar S. Niknafs, Jean C-Y.Tien, Yasuyuki Hosono, Matthew K. Iyer, Sahr Yazdani, Shruthi Subramanyiam, Sudhanshu K. Shukla, Xia Jiang, Lisha Wang, Tzu-Ying Liu, Michael Uhl, Alexander Gawronski, Yuanyuan Qiao, Lanbo Xiao, Saravana M. Dhanasekaran, Kristin M. Juckette, Lakshmi P. Kunju, Xuhong Cao, Utsav Patel, Mona Batish, Girish C. Shukla, Michelle T. Paulsen, Mats Ljungman, Hui Jiang, Rohit Mehra, Rolf Backofen, Cenk S. Sahinalp, Sue Freier, Andy Watt, Shuling Guo, John T. Wei, Felix Y. Feng, Rohit Malik[#], Arul M. Chinnaiyan[#]. **Analysis of the androgen receptor-regulated lncRNA landscape identifies a role for ARLNC1 in prostate cancer progression.** *Nature Genetics*, May 28, 2018, doi: 10.1038/s41588-018 -0120-1 (ARLNC1 is another name for PRCAT47)

Analysis of the androgen receptor–regulated lncRNA landscape identifies a role for ARLNC1 in prostate cancer progression

Yajia Zhang[1,2,3,4,23], Sethuramasundaram Pitchiaya[1,2,23], Marcin Cieślik[1,2,23], Yashar S. Niknafs[1,5], Jean C.-Y. Tien[1,2], Yasuyuki Hosono[1], Matthew K. Iyer[1,4], Sahr Yazdani[1], Shruthi Subramaniam[1], Sudhanshu K. Shukla[1,20], Xia Jiang[1], Lisha Wang[1], Tzu-Ying Liu[6], Michael Uhl[7], Alexander R. Gawronski[8], Yuanyuan Qiao[1,2,9], Lanbo Xiao[1], Saravana M. Dhanasekaran[1,2], Kristin M. Juckette[1], Lakshmi P. Kunju[1,2,9], Xuhong Cao[1,10], Utsav Patel[11], Mona Batish[11,12], Girish C. Shukla[13], Michelle T. Paulsen[9,14], Mats Ljungman[9,14], Hui Jiang[6,9], Rohit Mehra[2,9,15], Rolf Backofen[7], Cenk S. Sahinalp[16,17], Susan M. Freier[18], Andrew T. Watt[18], Shuling Guo[18], John T. Wei[15], Felix Y. Feng[1,9,14,19,21], Rohit Malik[1,22,24] and Arul M. Chinnaiyan[1,2,4,5,9,10,15,24]*

The androgen receptor (AR) plays a critical role in the development of the normal prostate as well as prostate cancer. Using an integrative transcriptomic analysis of prostate cancer cell lines and tissues, we identified ARLNC1 (AR-regulated long noncoding RNA 1) as an important long noncoding RNA that is strongly associated with AR signaling in prostate cancer progression. Not only was ARLNC1 induced by the AR protein, but ARLNC1 stabilized the *AR* transcript via RNA–RNA interaction. ARLNC1 knockdown suppressed AR expression, global AR signaling and prostate cancer growth in vitro and in vivo. Taken together, these data support a role for ARLNC1 in maintaining a positive feedback loop that potentiates AR signaling during prostate cancer progression and identify ARLNC1 as a novel therapeutic target.

L ong noncoding RNAs (lncRNAs) are a class of transcripts with diverse and largely uncharacterized biological functions[1–3]. Through crosstalk with chromatin, DNA, RNA species and proteins, lncRNAs function via chromatin remodeling, as well as transcriptional and post-transcriptional regulation[4–9]. High-throughput RNA sequencing (RNA-seq) has enabled the identification of lncRNAs with suggested oncogenic and tumor-suppressive roles, including involvement in the pathogenesis of prostate cancer[7,10–12]. Primary prostate cancer is often hormone dependent and relies on signaling through the AR; therefore, the majority of patients are responsive to front-line treatment with androgen-deprivation therapy[13–15]. However, approximately 20% of cases progress to an incurable stage of the disease known as castration-resistant prostate cancer (CRPC), which still critically relies on AR signaling[16,17],

as evidenced by the clinical benefit afforded through the use of enzalutamide[18–21] or abiraterone[22–24]. While substantial efforts have been undertaken to identify mechanisms of sustained AR signaling in CRPC (i.e., AR alterations, *AR* splice variants and alternative activation pathways)[25–31], few studies have investigated the role of AR-regulated lncRNAs. Therefore, we initiated a comprehensive RNA-seq profiling investigation of AR-regulated, cancer-associated lncRNAs from prostate cancer cell lines and patient tissue samples.

Results

Analysis of AR-regulated transcriptome in prostate cancer. To nominate AR-regulated genes (ARGs), RNA-seq was performed on AR-dependent VCaP and LNCaP prostate cancer cell lines that were stimulated with an AR ligand, dihydrotestosterone (DHT), for 6 and

Fig. 1 | Identification of AR-regulated genes in prostate cancer. a, The androgen-regulated transcriptome of prostate cancer cells. The heat map represents the 1,702 genes (including 547 lncRNAs) differentially regulated in LNCaP and VCaP cells following 6 and 24 h of DHT treatment. **b**, The landscape of transcriptomic alterations of prostate cancer progression. The heat map depicts 1,155 protein-coding genes and 547 lncRNAs across benign prostate (normal, $n = 52$ samples), localized prostate cancer (PCa, $n = 500$ samples) and metastatic prostate cancer (Mets, $n = 100$ samples) in TCGA prostate and SU2C-PCF RNA-seq data, with rows representing genes and columns representing patients. Patients were grouped by clinical stage, and genes were subjected to hierarchical clustering. Expression variability is quantified for each gene as a z-score relative to the mean expression in normal prostate samples. **c**, A heat map representation of ranked median gene expression levels in prostate tissues. Canonical prostate lineage and prostate cancer markers are listed.

24 h (Supplementary Fig. 1a). A total of 1,702 genes were identified to be concordantly induced or repressed in VCaP and LNCaP cells at both time points (Fig. 1a, Supplementary Fig. 1b,c and Supplementary Table 1), including more than 500 lncRNAs (Fig. 1a and Supplementary Fig. 1d); these data indicate that a large portion of the AR transcriptome remains uncharacterized.

To differentiate between direct and indirect ARGs, previously published and in-house AR chromatin immunoprecipitation (ChIP)–seq data from LNCaP and VCaP cells were analyzed[32]. As expected for direct AR targets, increased levels of AR binding at transcription start sites (TSSs) in both LNCaP and VCaP cells were observed (Supplementary Fig. 1e). The binding levels decreased following treatment with an AR antagonist (enzalutamide) (Supplementary Fig. 1f,g), and the binding sites revealed a de novo motif identical to the canonical AR response element[33] (Supplementary Fig. 1h). A total of 987 genes were categorized as direct ARGs, including 341 lncRNAs (lncARGs) (Supplementary Table 1). Within these genes, we observed an enrichment of chromatin marks associated with 'open' chromatin (H3K27ac, H3K4me1), active promoters (H3K4me3) and transcription (H3K36me3), which, together with RNA polymerase II (Pol II) occupancy, are recognized as manifestations of active gene expression (Supplementary Fig. 1i). Bromodomain and extra-terminal (BET) family proteins, such as BRD4, recognize acetylated

histones and have been shown to promote AR transcriptional activity[32]. Consistent with this, we observed colocalization of BRD4 and AR proteins at the promoters of direct AR-responsive genes and loss of AR ChIP peaks following treatment with a bromodomain inhibitor (JQ1) (Supplementary Fig. 1f,i). We further sought to determine whether ARGs identified from cell lines were also targeted by AR in normal prostate tissues and primary tumors. We leveraged a published dataset[34] and queried for the presence of AR peaks within ARG promoters. Remarkably, the majority of ARG promoters were TSS-proximally bound by AR in both tissues and cell lines (Supplementary Fig. 1j,k); conversely, AR-independent genes were distal to AR-binding sites (Supplementary Fig. 1l).

Finally, we confirmed that the ARGs were also expressed in human prostate tissues. We interrogated RNA-seq data from normal prostate, clinically localized prostate cancer (The Cancer Genome Atlas, TCGA)[35] and metastatic CRPC (Stand Up to Cancer–Prostate Cancer Foundation, SU2C-PCF)[30] (Fig. 1b). This revealed remarkable heterogeneity in the expression of ARGs during prostate cancer progression to metastatic disease. As expected, compared to protein-coding genes, noncoding ARGs were detected at lower overall levels (Fig. 1c), although ~10% showed robust expression of over 10 FPKM (fragments per kilobase of transcript per million mapped reads) on average across prostate cancer samples.
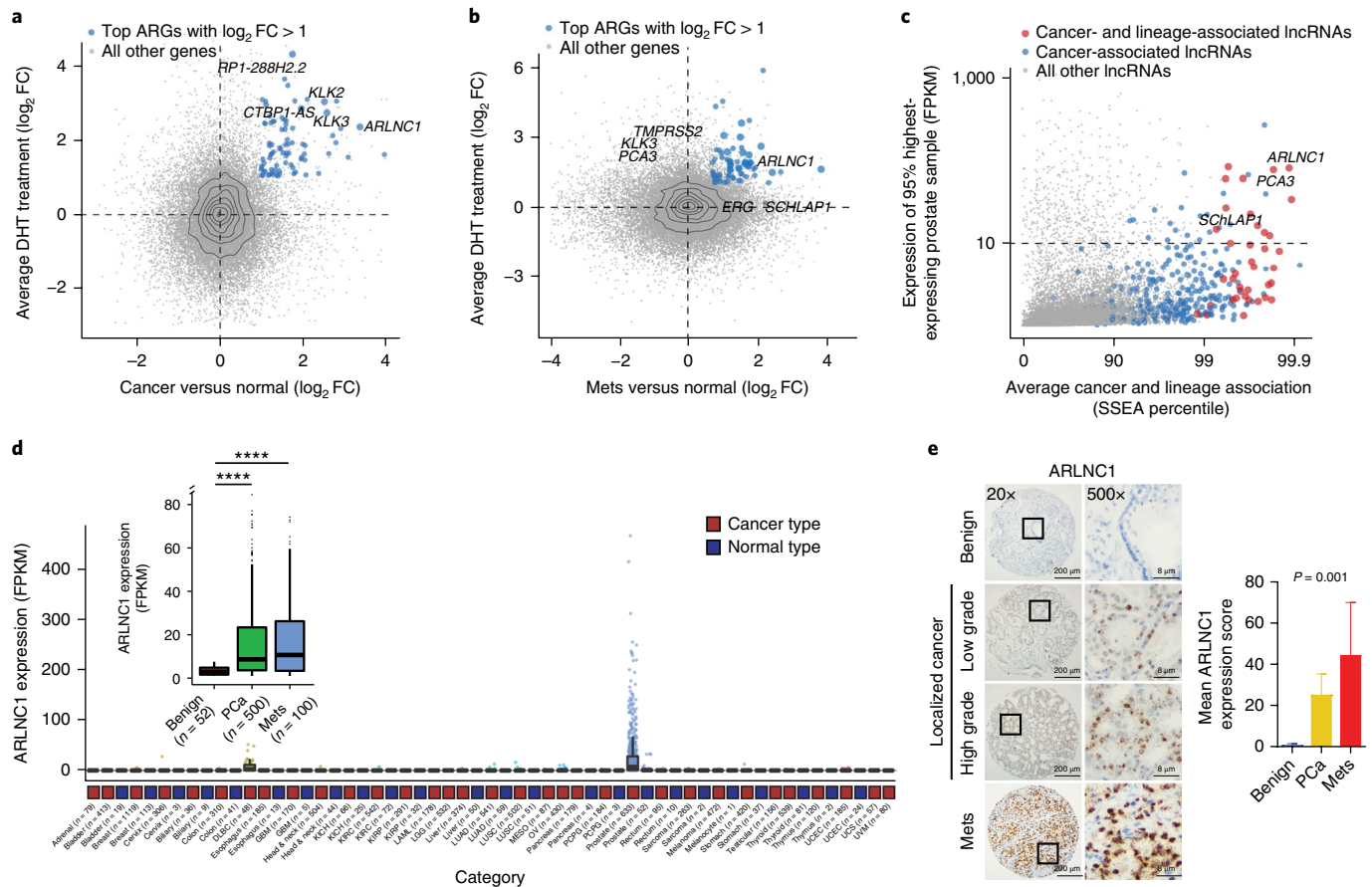
Fig. 2 | Nomination and in situ characterization of ARLNC1 in prostate cancer. a,b, Identification of androgen-regulated transcripts elevated in prostate cancer progression. Scatterplots show the AR regulation and cancer association of the ARGs identified in Fig. 1a. The y axis depicts the $\log_2$-transformed fold change in gene expression following DHT stimulation, and the x axis indicates the $\log_2$-transformed difference in gene expression level between benign prostate (n = 52 samples) and localized prostate cancer (n = 500 samples) (**a**) and between benign prostate (n = 52 samples) and metastatic prostate cancer (n = 100 samples) (**b**). Significant genes with $\log_2$ fold change > 1 were ranked according to combined P value (limma-moderated t test). **c**, Nomination of prostate cancer- and lineage-associated lncRNAs based on expression levels. The scatterplot shows the expression level, prostate tissue specificity and prostate cancer association of lncRNAs. The expression level is the FPKM value at the 95th percentile across TCGA prostate samples. Average cancer and lineage associations are represented by the percentile rank for each gene in SSEA (total n = 7,256 samples). **d**, Relative expression (FPKM) of ARLNC1 across different cancer types in the TCGA cohort. Inset, relative expression (FPKM) of ARLNC1 across benign prostate (n = 52 samples), localized prostate cancer (n = 500 samples) and metastatic prostate cancer (n = 100 samples). PCa versus Normal: ****$P < 2.2 \times 10^{-16}$; Mets versus Normal: ****$P = 2.6 \times 10^{-7}$ (two-sided t test). Box-plot definitions: the center line depicts the median, the box shows the first and third quartiles, and the whiskers follow the 1.5 rule. **e**, ISH of ARLNC1 transcript in a human prostate cancer tissue microarray. Representative ARLNC1 staining is shown for benign prostate and localized and metastatic prostate cancer tissue. The bar plot represents mean ARLNC1 expression scores across benign prostate (n = 11), localized prostate cancer (n = 85) and metastatic prostate cancer (n = 37) tissues, with vertical bars indicating the bootstrapped 95% confidence interval of the means. Significance was calculated by a Kruskal–Wallis rank-sum test.

ARLNC1 is a prostate lineage-specific lncRNA with elevated expression in cancer. We hypothesized that lncRNAs associated with prostate cancer progression and castration resistance should be either upregulated if they enhance AR signaling or, conversely, downregulated if they attenuate AR signaling. Their expression is also expected to be AR dependent and lineage restricted if they are part of bona fide physiological feedback loops. Accordingly, a top–down strategy was developed to establish and prioritize clinically relevant, prostate cancer- and lineage-specific lncARGs. First, we identified genes that were both regulated by AR in the VCaP and LNCaP cell lines and upregulated in primary (Fig. 2a) or metastatic (Fig. 2b) prostate cancer as compared to normal prostate tissues. As expected, canonical AR targets, including KLK3, KLK2 and TMPRSS2, were among the most differentially expressed protein-coding genes. Notably, this approach highlighted several novel lncARGs, including ARLNC1

(ENSG00000260896, PRCAT47[10]), and validated previously identified lncARGs, such as CTBP1-AS[36] (Fig. 2a,b). Interestingly, ARLNC1 was found to be one of the most differentially expressed AR-regulated genes in both localized and metastatic prostate cancer (Fig. 2a,b and Supplementary Fig. 2a,b).

Next, we sought to establish the prostate lineage and cancer specificity of prostate cancer–associated lncRNAs. We leveraged the MiTranscriptome assembly[10], an online resource, to interrogate lncRNA expression across a multitude of tissue and tumor types, and we calculated sample set enrichment analysis (SSEA) scores, which indicate the strength of cancer and lineage association[10]. After applying an expression-level filter (10 FPKM at the 95th percentile), we identified 12 of the most prostate lineage- and cancer-specific lncRNAs (Fig. 2c and Supplementary Fig. 2c,d); 5 of these lncRNAs were regulated by AR. Across these analyses, ARLNC1 was the top prioritized transcript and thus warranted further investigation.
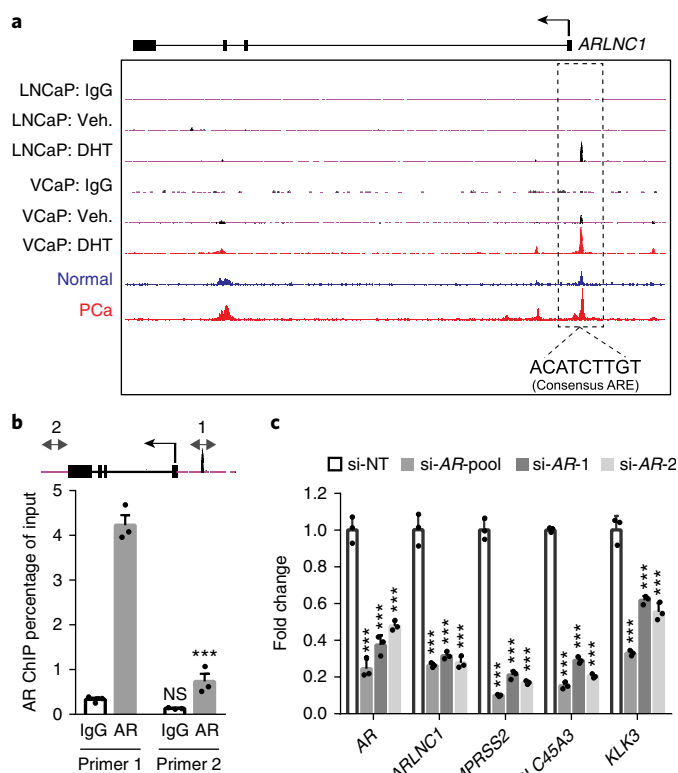
Fig. 3 | ARLNC1 is directly regulated by AR. a, AR ChIP–seq in prostate cancer cell lines and tissues. Normalized ChIP–seq enrichment is shown. Top, AR or control (IgG) ChIP–seq results across the *ARLNC1* locus in LNCaP and VCaP cells with vehicle (ethanol) or DHT treatment. Bottom, AR ChIP–seq in benign prostate and clinically localized prostate cancer tissue. ARE, androgen response element. **b**, ChIP–qPCR in MDA-PCa-2b cells showing AR or IgG enrichment (ChIP/input) over the *ARLNC1* promoter region (primer 1) or a control region (primer 2). Data are shown as the mean ± s.e.m. (*n* = 3 biologically independent samples). ***P (adjusted) < 0.0001, NS (not significant): *P* = 0.5746, compared to the control region (primer 2) by ANOVA with Sidak correction for multiple comparisons. Top, schematic of the amplicon locations for ChIP–qPCR validation. **c**, Expression of *AR* and AR target genes (*ARLNC1*, *TMPRSS2*, *SLC45A3* and *KLK3*) in MDA-PCa-2b cells transfected with control siRNA (si-NT) or siRNAs against *AR* (si-*AR*-pool, si-*AR*-1, si-*AR*-2). Mean ± s.e.m. values are shown, *n* = 3 biologically independent samples. ***P = 0.0001, determined by ANOVA with Dunnett's multiple-comparisons test.

Expression of ARLNC1 was interrogated across cancer and normal tissue RNA-seq samples from TCGA and the Genotype-Tissue Expression (GTEx) project[37,38], respectively. In the TCGA cohort, ARLNC1 exhibited a highly prostate cancer–specific expression pattern, with little to no expression in other tumor types (Fig. 2d). Similarly, in the GTEx normal tissue cohort, its expression was limited to the prostate (Supplementary Fig. 2e). Among the prostate samples, ARLNC1 expression was significantly higher in localized and metastatic prostate cancers than in benign tissues, as assessed by RNA-seq (Fig. 2d, inset) and in situ hybridization (ISH; Fig. 2e). In an extensive differential expression analysis using MiTranscriptome, ARLNC1 was found to be among the top 1% of transcripts most upregulated in prostate cancer and specific to the prostate lineage, with no significant associations in other tissues (Supplementary Fig. 2f). Moreover, the protein-coding genes that were most correlated with ARLNC1 were found to be associated with prostate cancer progression in ONCOMINE concept analyses performed on multiple clinical datasets[39] (Supplementary Fig. 2g). Together, these

results confirm that ARLNC1 expression is restricted to the prostate lineage, elevated in prostate cancer and associated with AR signaling throughout prostate cancer progression.

To functionally characterize ARLNC1, we first identified appropriate prostate cancer cell lines with moderate to high levels of ARLNC1 expression using in-house RNA-seq data (Supplementary Fig. 3a). Supporting the association of AR with ARLNC1, ARLNC1 expression was highly enriched in AR-positive cell lines, with the highest expression in MDA-PCa-2b and LNCaP cells. In addition, qPCR analysis for the ARLNC1 transcript also demonstrated that this gene was expressed at the highest level in the MDA-PCa-2b and LNCaP cell lines (Supplementary Fig. 3b). As existing annotations of the *ARLNC1* gene (located on chromosome 16) predict the presence of several transcript isoforms that differ in exon and TSS usage, we determined the exact structure in MDA-PCa-2b and LNCaP cells by RACE. A common TSS for *ARLNC1* was found in both cell lines, and the ~2.8-kb transcript isoform was further confirmed by northern blot analysis (Supplementary Fig. 3c). Single-molecule FISH (smFISH) revealed that approximately 100 molecules of ARLNC1 transcript existed per MDA-PCa-2b cell (Supplementary Fig. 3d,e). Using smFISH and qPCR, we also found that ARLNC1 molecules were distributed equally between the nuclear and cytoplasmic cellular compartments (Supplementary Fig. 3f,g).

ARLNC1 transcription is directly regulated by AR. Because ARLNC1 was identified as an AR-regulated lncRNA, we inspected the promoter region of the *ARLNC1* gene for AR occupancy and identified an androgen-induced AR peak in AR ChIP-seq data from both DHT-stimulated VCaP and LNCaP cells (Fig. 3a). Notably, this AR-binding site was also observed in prostate tissue samples and contained a canonical androgen response element[33] (Fig. 3a). These observations were corroborated by ChIP–qPCR in MDA-PCa-2b cells, which showed the highest level of ARLNC1 expression (Fig. 3b). Considering the observation that ARLNC1 expression is prostate tissue specific, while AR expression is not as much, we searched for additional regulators (transcription factors and epigenetic modifiers) of the *ARLNC1* gene (Supplementary Fig. 4a). Motif analysis of the *ARLNC1* promoter region identified several transcription factor binding sites, including a FOXA1 response element. To further validate *ARLNC1* gene regulation by AR and FOXA1, we evaluated ARLNC1 transcript levels following AR or FOXA1 knockdown. AR or FOXA1 loss resulted in decreased expression of ARLNC1, along with other canonical AR target genes that served as positive controls (Fig. 3c and Supplementary Fig. 4b). ChIP–seq and ChIP–qPCR analyses additionally confirmed the putative FOXA1-binding motif on the *ARLNC1* promoter (Supplementary Fig. 4c). Together, these observations suggest that ARLNC1 is directly regulated by AR and modestly regulated by FOXA1, which partially explains the tissue-specific expression pattern of ARLNC1, as expression of these two transcription factors overlaps nearly exclusively in prostate tissue[37,38] (Supplementary Fig. 4d).

ARLNC1 regulates AR signaling. To elucidate the function of ARLNC1 in prostate cancer, we performed gene expression profiling of wild-type and ARLNC1-knockdown MDA-PCa-2b cells (Fig. 4a). Gene ontology (GO) pathway enrichment analysis of the differentially expressed genes revealed deregulation of four main biological activities: apoptosis, cell proliferation, DNA damage response and androgen signaling (Fig. 4a). The significant decrease in AR target gene expression is particularly interesting given the fact that ARLNC1 is regulated by AR, suggesting a positive feedback loop between ARLNC1 and AR signaling. To confirm this observation, we generated an AR target gene signature from MDA-PCa-2b cells stimulated with DHT (Supplementary Fig. 5a and Supplementary Table 2) and performed gene set enrichment analysis (GSEA) using this gene signature (Fig. 4b). Knockdown
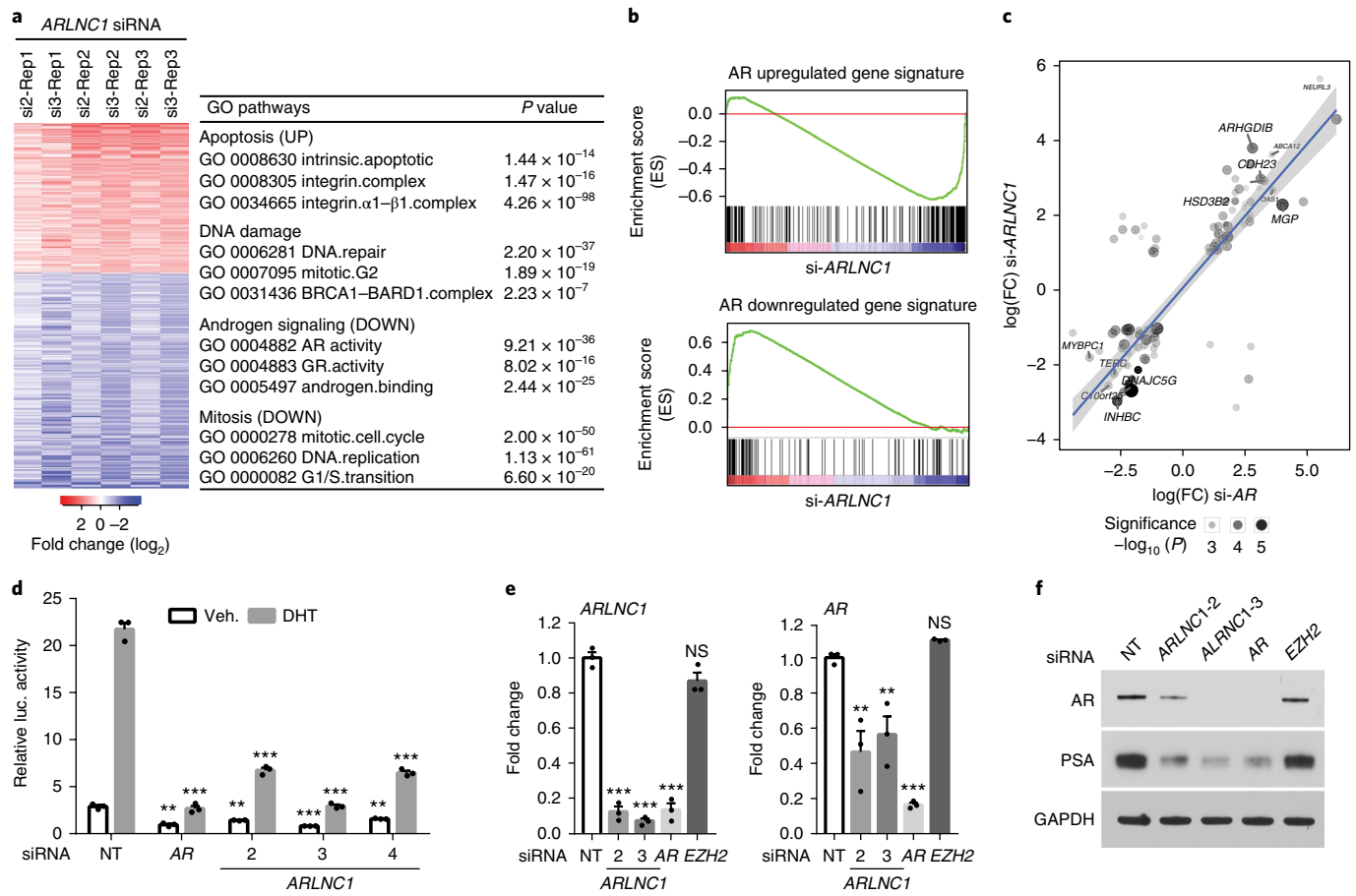
Fig. 4 | ARLNC1 loss attenuates AR signaling. a, Gene expression profiling for ARLNC1 knockdown in MDA-PCa-2b cells ($n = 3$ biologically independent cell cultures for each siRNA). The chart presents the top enriched pathways following ARLNC1 knockdown, identified using GO enrichment analysis (RandomSet test). **b**, GSEA showing significant enrichment of the ARLNC1-regulated gene set with respect to the AR target gene sets ($n = 3$ independent gene expression profiles). Shown are enrichment plots for gene sets consisting of genes positively regulated by AR (top) and genes negatively regulated by AR (bottom). **c**, Comparison of ARLNC1-regulated and AR target genes based on RNA–seq following knockdown of AR and ARLNC1. Significant genes and their log-transformed fold changes in either of the conditions are shown ($n = 2$ independent cell cultures per-condition). Combined significance levels, determined by a limma-moderated t test (across both knockdowns), are indicated by circle size. **d**, siRNA knockdown of *ARLNC1* in MDA-PCa-2b cells impairs AR signaling as determined by AR reporter gene assay. siRNA against *AR* serves as a positive control for inhibition of AR signaling. Mean ± s.e.m. values are shown, $n = 3$ biologically independent cell cultures. **$P < 0.01$, ***$P = 0.0001$, determined by ANOVA with Dunnett correction. **e**, qRT-PCR analysis of *ARLNC1* and *AR* in MDA-PCa-2b cells transfected with siRNAs against *ARLNC1*, *AR*, *EZH2* or non-specific control (NT). siRNA against *AR* serves as a positive control for inhibition of AR signaling, while siRNA against *EZH2* serves as a negative control. Mean ± s.e.m. values are shown, $n = 3$. **$P < 0.01$, ***$P = 0.0001$, determined by ANOVA with Dunnett correction. **f**, Immunoblots of AR, PSA and GAPDH in MDA-PCa-2b cells transfected with siRNAs against *ARLNC1*, *AR*, *EZH2* or non-specific control (NT). The experiments were repeated three times independently with similar results. Uncropped images are shown in Supplementary Fig. 9.

of ARLNC1 led to suppression of genes positively regulated by AR and upregulation of genes negatively regulated by AR (Fig. 4b,c and Supplementary Fig. 5b). This was further confirmed by an AR reporter activity assay (Fig. 4d and Supplementary Fig. 5c), as well as qPCR analysis of AR target genes (Supplementary Fig. 5d). Interestingly, ARLNC1 knockdown also had a significant effect on the mRNA and protein levels of AR (Fig. 4e,f), suggesting direct regulation of AR by ARLNC1. However, we found that ARLNC1 overexpression did not affect AR and its signaling cascade (Supplementary Fig. 5e).

In situ colocalization of ARLNC1 and *AR* transcripts. Noncoding RNAs have been shown to target mRNAs via direct or indirect RNA–RNA interaction[9,40–42]. To identify target mRNAs that could interact with ARLNC1, we performed unbiased prediction of RNA–RNA interactions using IntraRNA[43,44]. Interestingly, the 3′ UTR of the *AR* transcript was identified as a target of ARLNC1

(Fig. 5a and Supplementary Fig. 6a). An in vitro RNA–RNA interaction assay between the 3′ UTR of *AR* and full-length ARLNC1 confirmed this in silico prediction (Fig. 5b). To evaluate this interaction in the context of the cellular environment, multiplexed smFISH for *AR* and ARLNC1 transcripts was performed in MDA-PCa-2b cells. On co-staining of MDA-PCa-2b cells for either a combination of *AR* transcripts and a panel of lncRNAs or ARLNC1 and a panel of mRNAs, we observed specific colocalization of *AR* and ARLNC1 transcripts in the nucleus within foci that were typically larger than individual molecules (Fig. 5c–e). The extent of colocalization was much higher than that expected from coincidental colocalization with an abundant transcript, such as MALAT1 or *GAPDH* (Fig. 5c–e). More specifically, colocalization typically occurred at a stoichiometry of 2:1 ARLNC1/*AR*, which accounted for ~10–20% of all *AR* and ARLNC1 transcripts in the cell (Supplementary Fig. 6b). Furthermore, *AR*–ARLNC1 colocalization was observed in *ARLNC1*-positive prostate cancer tissues (Fig. 5f,g).
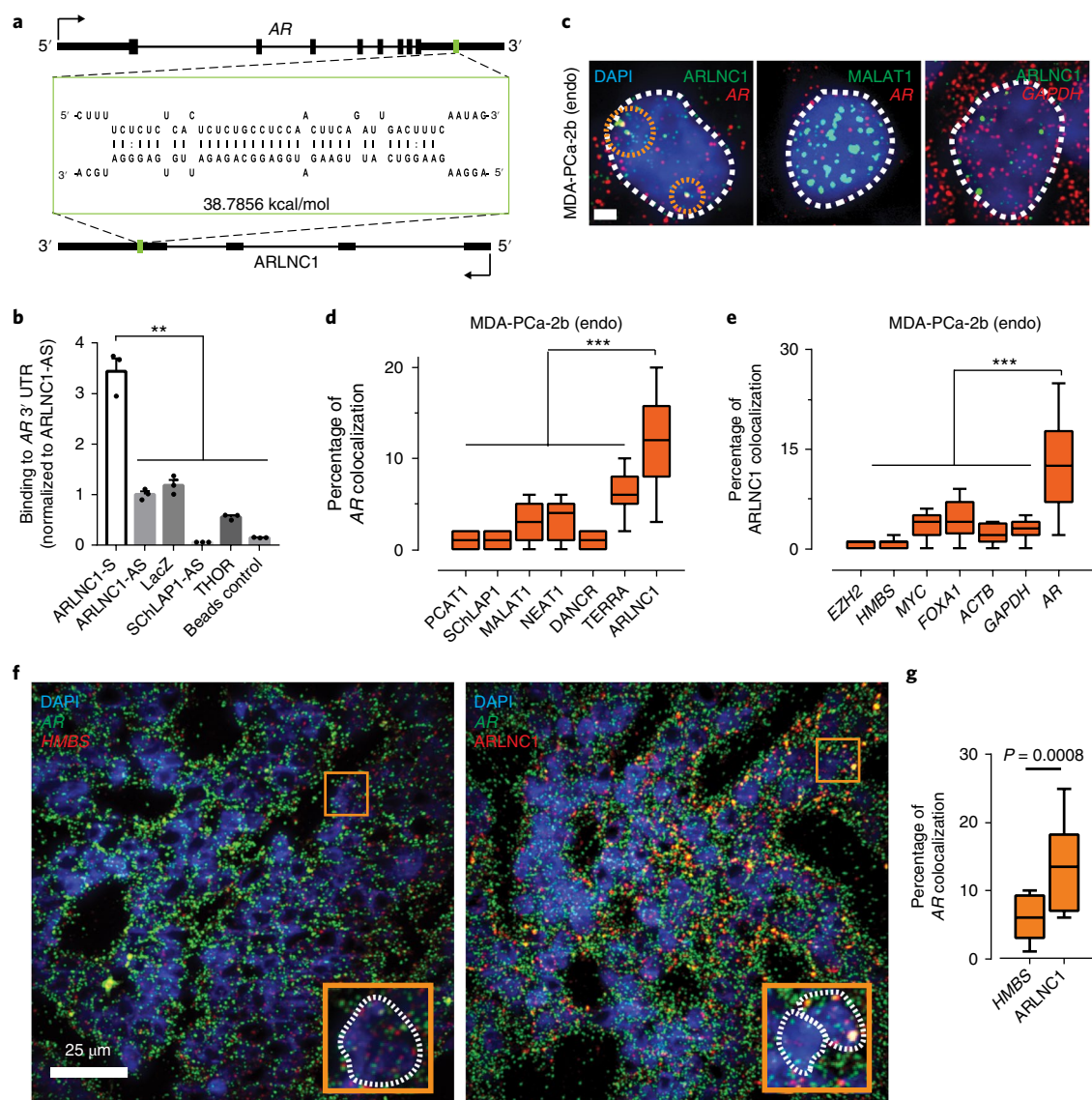
Fig. 5 | In situ colocalization of *AR* mRNA and ARLNC1 in prostate cancer cells. a, Schematic of the predicted RNA–RNA interaction between ARLNC1 and the 3′ UTR of *AR*. **b**, ARLNC1 interacts with the *AR* 3′ UTR in an in vitro RNA–RNA interaction assay. Compared to a panel of control RNAs (ARLNC1 antisense, LacZ, SChLAP1-AS, THOR), ARLNC1 binds to *AR* 3′ UTR-1–980 with high affinity. The binding affinity was quantified by qPCR analysis of the *AR* 3′ UTR. Data were normalized to the ARLNC1-AS control. Mean ± s.e.m. are shown, $n = 3$. **$P < 0.001$, by two-tailed Student's t test. **c–e**, smFISH depiction of *AR*–ARLNC1 colocalization in situ. **c**, Representative pseudocolored images of MDA-PCa-2b cell nuclei stained for the appropriate endogenous (endo) transcripts (green, red) and with DAPI (nucleus, blue). Scale bar, 5 μm. The orange circles represent regions of colocalization. **d,e**, Quantification of the percentage of *AR* or ARLNC1 molecules colocalizing with a panel of lncRNAs (**d**) or mRNAs (**e**). The center line and whiskers depict the median and range, respectively, and the box extends from the 25th to the 75th percentile ($n = 50$ cells for each sample aggregated from 3 independent experiments). ***$P < 0.0001$, by two-tailed Student's t test. **f**, Representative pseudocolored images of ARLNC1-positive prostate cancer tissues stained with DAPI (nucleus, blue) and for *AR* (green), *HMBS* (red) or ARLNC1 (red) transcripts (smFISH). Inset, 5.5 × 5.5 μm² zoomed-in view of the box within the main panel. **g**, Quantification of the percentage of *AR* molecules colocalizing with *HMBS* transcripts or ARLNC1. The center line and whiskers depict the median and range, respectively, and the box extends from the 25th to the 75th percentile ($n = 15$ field-of-views for each sample aggregated from 3 independent tissues). $P < 0.001$, by two-tailed Student's t test.

Using an in vitro RNA–RNA binding assay, we identified nucleotides 700–1300 of ARLNC1 to be critical for binding to the *AR* 3′ UTR (Fig. 6a,b). To confirm this observation within the cellular context, we ectopically overexpressed different fragments of ARLNC1 together with *AR* in U2OS osteosarcoma cells. In this exogenous system, colocalization of *AR* and ARLNC1 was once again demonstrated, wherein colocalization was dependent on the presence of nucleotides 700–1300 of ARLNC1 (Fig. 6c,d and Supplementary Fig. 6c). Furthermore, incubation with antisense oligonucleotides (ASOs) that blocked the interaction site led to a

significant reduction in ARLNC1–*AR* interaction in vitro and in situ (Fig. 6e,f and Supplementary Fig. 6d,e). Decreased AR signaling was also observed following blocking of this interaction (Fig. 6g and Supplementary Fig. 6f).

ARLNC1 regulates the cytoplasmic levels of *AR* transcripts. We then sought to delineate the mechanism of ARLNC1-mediated AR regulation. We first monitored the stability of these two transcripts and found that *AR* and ARLNC1 have similar half-lives of ~9 h (Supplementary Fig. 6g). As ARLNC1 depletion resulted in a
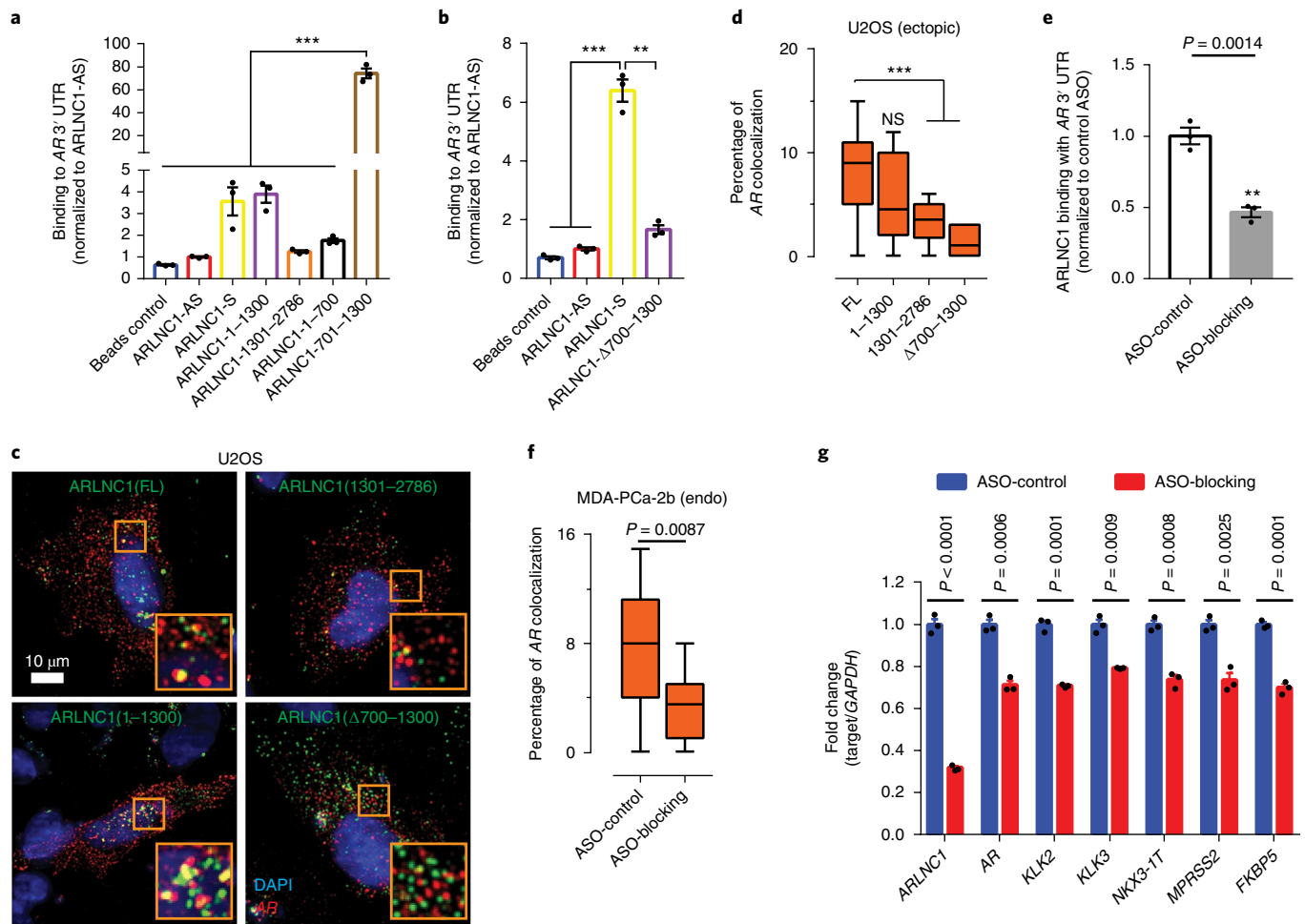
Fig. 6 | Identification of the ARLNC1 fragment mediating RNA–RNA interaction with *AR* mRNA. a, In vitro RNA–RNA interaction assay identifies nucleotides 700–1300 on ARLNC1 as critical binding site to *AR* 3′ UTR-1–980. ARLNC1 fragments covering nucleotides 700–1300 display comparable or higher *AR* 3′ UTR binding affinity than ARLNC1-S, with ARLNC1-700–1300 exhibiting the highest binding affinity. Data were normalized to the ARLNC1-AS control. Mean ± s.e.m. values are shown, *n* = 3. ***P (adjusted) = 0.0001, determined by ANOVA with Dunnett's multiple-comparisons test. **b**, Deletion of nucleotides 700–1300 on ARLNC1 results in impaired binding to the *AR* 3′ UTR, as shown by in vitro RNA–RNA interaction assay. Data were normalized to the ARLNC1-AS control. Mean ± s.e.m. values are shown, *n* = 3. ***P = 0.0001, **P = 0.0003, by two-tailed Student's *t* test. **c,d**, smFISH shows that nucleotides 700–1300 in ARLNC1 are important for colocalization in situ. **c**, Representative pseudocolored images of U2OS cells stained with DAPI (nucleus, blue) and for ARLNC1 (green) and *AR* transcripts (red). Inset, 10 × 10 μm² zoomed-in view of the orange box in the main image. **d**, Quantification of the percentage of *AR* molecules colocalizing with various ARLNC1 fragments. The center line and whiskers depict the median and range, respectively, and the box extends from the 25th to the 75th percentile (*n* = 50 cells for each sample aggregated from 3 independent experiments). ***P < 0.0001, by two-tailed Student's *t* test. NS, not significant. **e**, ASOs targeting nucleotides 700–1300 on the ARLNC1 transcript (ASO-blocking pool) inhibit ARLNC1 interaction with the *AR* 3′ UTR. In vitro RNA–RNA interaction assays were performed using ARLNC1 and the *AR* 3′ UTR, with the addition of the blocking ASO pool or control ASO. Data were normalized to the control ASO. Mean ± s.e.m. values are shown, *n* = 3. P = 0.0014, by two-tailed Student's *t* test. **f**, smFISH shows that ASOs targeting nucleotides 700–1300 on the ARLNC1 transcript (ASO-blocking) inhibit ARLNC1 colocalization with *AR* in situ. Quantification is shown of the percentage of *AR* transcripts colocalizing with ARLNC1 after various treatments in MDA-PCa-2b cells. The center line and whiskers depict the median and range, respectively, and the box extends from the 25th to the 75th percentile (*n* = 50 cells for each sample aggregated from 3 independent experiments). The P value was computed by two-tailed Student's *t* test. **g**, qPCR analysis of *ARLNC1*, *AR* and AR signaling genes (*KLK2*, *KLK3*, *NKX3-1*, *TMPRSS2* and *FKBP5*) in MDA-PCa-2b cells transfected with control or blocking ASOs targeting the interaction site between ARLNC1 and the *AR* 3′ UTR. Mean ± s.e.m. values are shown, *n* = 3. Significance was determined by two-tailed Student's *t* test.

striking reduction of AR protein levels, much more than could be explained by *AR* transcript reduction, we hypothesized that ARLNC1 could affect *AR* post-transcriptionally. To test this hypothesis, we tracked the subcellular localization of *AR* transcripts using smFISH after depleting ARLNC1. We confirmed successful in situ knockdown of ARLNC1 using siRNAs, antisense oligonucleotide (ASO) and the blocking oligonucleotides that targeted the ARLNC1–*AR* interaction (ASO-blocking) in MDA-PCa-2b cells (Supplementary Fig. 6h,i). Quantification of the subcellular distribution of ARLNC1

suggested that the nuclear fraction of ARLNC1 was enriched only in the *ARLNC1* siRNA (si-*ARLNC1*) condition (Supplementary Fig. 6j), a result expected for siRNAs that are typically more functional in the cytosol[45]. Surprisingly, ARLNC1 knockdown or obstruction of the *AR*–ARLNC1 interaction increased the nuclear *AR* fraction by dramatically decreasing cytoplasmic levels of the *AR* transcript (Fig. 7a,b and Supplementary Fig. 6k–l). This observation was further supported by BrU-seq and BrUChase-seq, two high-throughput tools that monitor transcript synthesis and stability. On ARLNC1
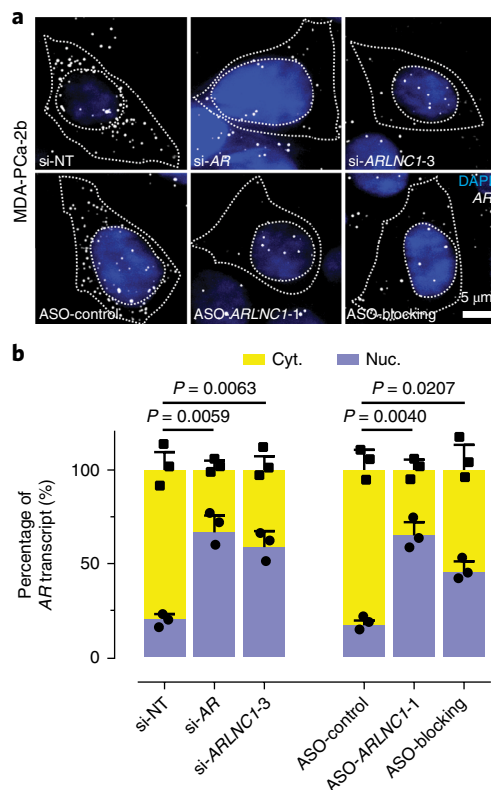
Fig. 7 | ARLNC1 regulates the cytoplasmic level of the *AR* transcript.
a, ARLNC1 regulates *AR* post-transcriptionally by specifically affecting cytoplasmic *AR* mRNA. Representative pseudocolored images are shown of MDA-PCa-2b cells stained for DAPI (nucleus, blue) and *AR* (gray) after treatment with siRNA against *AR* (si-*AR*), siRNA against *ARLNC1* (si-*ARLNC1*-3), ASO against *ARLNC1* (ASO-*ARLNC1*-1) or blocking ASO against the *AR*–ARLNC1 colocalizing segment (ASO-blocking). Quantification of knockdown is shown in Supplementary Fig. 6k,l. **b**, Fractional column plots depicting the nucleo-cytoplasmic distribution of *AR* mRNA after the various treatment conditions in **a**, as computed using smFISH. Mean ± s.e.m. values are shown, $n = 3$ independent experiments and 60 cells analyzed for each sample. The P values were computed by comparing to si-NT- or ASO-control-treated cells, by two-tailed Student's t test.

knockdown, the synthesis rate of the *AR* transcript remained the same (Supplementary Fig. 6m), while the stability of the transcript decreased, particularly through the 3′ UTR (Supplementary Fig. 6n). Taken together, our data suggest that ARLNC1 regulates the cytoplasmic levels of *AR* transcripts. Furthermore, the transcriptional coupling between *AR* and ARLNC1 transcripts is mediated by direct interactions that are encoded in their sequences.

Inhibition of ARLNC1 delays prostate cancer growth in vitro and in vivo. Having established a role for ARLNC1 in the regulation of AR signaling, we further evaluated the biological effects of ARLNC1 in prostate cancer cell lines. GO pathway enrichment analysis of the knockdown microarray data showed that ARLNC1-regulated genes were involved in cell proliferation and apoptosis (Fig. 4a). Knockdown of ARLNC1 had a significant effect on the proliferation of AR-dependent MDA-PCa-2b and LNCaP cells, but had no effect on AR-negative DU145 and PC3 cells (Fig. 8a and Supplementary Fig. 7a,b). Knockdown of ARLNC1 also resulted in increased apoptosis in AR-positive prostate cancer cells (Fig. 8b and Supplementary Fig. 7c). Notably, these results translated to effects in vivo, as cells expressing shRNA targeting *ARLNC1* formed smaller tumors in mice when compared to cells expressing non-targeting

shRNA (Fig. 8c), thus suggesting that ARLNC1 is an important survival factor for AR-dependent prostate cancer.

Because modulation of ARLNC1 expression levels resulted in a striking proliferation phenotype, we hypothesized that ARLNC1 inhibition could be used therapeutically for the treatment of prostate cancer. ASOs have recently been shown to be effective in targeting RNA in vivo[46–49]; thus, we designed ASOs targeting the ARLNC1 transcript (Supplementary Fig. 7d). Transfection of ASOs resulted in strong knockdown efficiency (Supplementary Fig. 7e), and ASO-mediated knockdown resulted in similar effects on gene expression profiling to siRNA (Fig. 8d,e and Supplementary Fig. 7f). Furthermore, AR-positive cells transfected with *ARLNC1* ASOs exhibited retarded growth, similar to those treated with siRNAs (Fig. 8f). To evaluate the therapeutic potential of *ARLNC1* ASOs in vivo, we first assessed the cellular free-uptake efficiency of *ARLNC1* ASOs, a prerequisite for ASO therapeutic use. Notably, several ASOs significantly reduced ARLNC1 levels through free uptake (Supplementary Fig. 7g). Free uptake of *ARLNC1* ASOs led to a significant decrease in the proliferation capacity of MDA-PCa-2b cells in both normal cell culture and 3D sphere conditions (Supplementary Fig. 7h–j). Treatment of mice bearing MDA-PCa-2b xenografts with *ARLNC1*-targeting ASOs led to significant decreases in tumor growth compared to control ASO (Fig. 8g,h and Supplementary Fig. 8a–e). Taken together, these data, along with the association of ARLNC1 with aggressive androgen signaling (Supplementary Fig. 8f–j), suggest that ARLNC1 plays a critical role in the proliferation of AR-dependent prostate cancer and can be effectively exploited as a therapeutic target.

Discussion
As AR signaling remains a significant driver of CRPC pathogenesis, it is imperative to generate novel strategies to target this pathway. Even with the addition of enzalutamide or abiraterone to CRPC treatment regimens, progression invariably occurs. Exploiting players other than AR itself that are pivotal to maintaining the magnitude of the androgen response is an alternative approach. Our comprehensive profiling of AR-regulated, prostate cancer–associated lncRNAs identified the top-ranking candidate ARLNC1 that we functionally characterized. We identified a positive feedback loop between ARLNC1 and AR that maintains the androgen transcriptional program in AR-positive prostate cancer cells, specifically through regulating the cellular levels of AR (Fig. 8i). The mechanism we identified echoes previous studies on lncRNAs—1/2-sbsRNAs[42], BACE1-AS[9] and TINCR[41], which highlights the role of lncRNA in increasing or decreasing RNA stability.

As a novel noncoding regulator of AR signaling, ARLNC1 has the potential to be not only a mechanistic biomarker but also a therapeutic target for advanced prostate cancer. In addition, the fact that it acts upstream of AR signaling presents the possibility that targeting ARLNC1 may afford an additional option to patients that have de novo or acquired resistance to therapies targeting AR itself (that is, enzalutamide or abiraterone). Furthermore, specific antisense nucleotides targeting ARLNC1, which we demonstrate to be specifically expressed in the prostate, could circumvent undesirable side effects that occur in other tissues with exposure to androgen synthesis inhibitors or anti-androgens.

Although we have identified a new node of the AR signaling network that can be therapeutically targeted, the molecular mechanism through which ARLNC1 regulates *AR* transcript levels remains to be fully characterized. At this time, it is unclear whether the physical interaction between the *AR* 3′ UTR and ARLNC1 functions with the aid of additional RNA-binding proteins (for example, HuR) and/or RNAs in vivo[50,51]. Nonetheless, the application of ASOs has ushered in an exciting era that makes it possible to target previously 'undruggable' molecules directly at the transcript level, such as ARLNC1, which is likely to yield promising opportunities in cancer treatment.
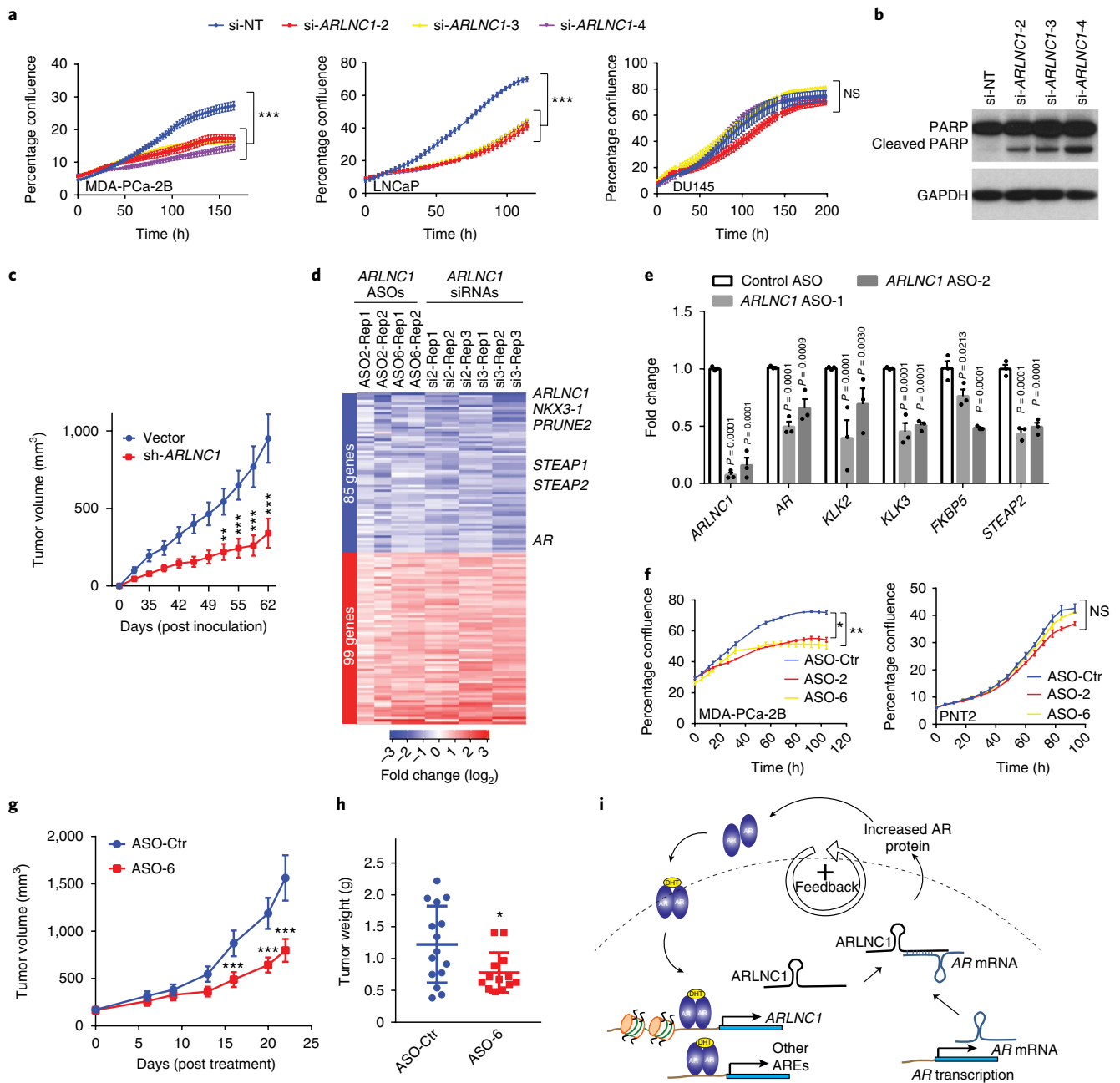
Fig. 8 | ARLNC1 as a therapeutic target in AR-positive prostate cancer models. a, siRNA-mediated knockdown of ARLNC1 in vitro in AR-positive prostate cancer cell lines (MDA-PCa-2b and LNCaP) inhibits cell proliferation. The AR-negative prostate cell line DU145 serves as a negative control. Mean ± s.d. values are shown, $n = 6$ independent cell cultures per group, **P (adjusted) $= 0.0001$ compared to si-NT-treated cells, by one-way ANOVA with Dunnett's multiple-comparisons test; NS, not significant. **b**, ARLNC1 loss leads to increased apoptosis as shown by western blot analysis of PARP and cleaved PARP in LNCaP cells following ARLNC1 knockdown. The experiment was repeated independently three times with similar results. Uncropped images are shown in Supplementary Fig. 9. **c**, Tumor growth of LNCaP-AR cells expressing shRNA targeting *ARLNC1* or shRNA vector. Mean ± s.e.m. values are shown. $n = 10$ independent tumors, ***$P < 0.0001$, **$P = 0.0007$, as determined by two-tailed Student's t test. **d**, Gene expression profiling for siRNA-mediated or ASO-mediated ARLNC1 knockdown in MDA-PCa-2b cells. The numbers above the heat map represent the specific microarray replicates. **e**, qRT–PCR analysis of *ARLNC1*, *AR* and AR targets (*KLK2*, *KLK3*, *FKBP5* and *STEAP2*) in MDA-PCa-2b cells transfected with ASOs against *ARLNC1*. Data were normalized to a housekeeping gene, and the levels in control ASO-treated cells were set to 1. Mean ± s.e.m. values are shown, $n = 3$. Adjusted P values were determined by one-way ANOVA with Dunnett correction for multiple comparisons. **f**, Transfection of ASOs targeting *ARLNC1* in AR-positive MDA-PCa-2b cells inhibits cell proliferation. The AR-negative prostate cell line PNT2 serves as a negative control. Mean ± s.e.m. values are shown, $n = 6$ independent cell cultures per treatment group. *P (adjusted) $= 0.0112$, **P (adjusted) $= 0.0065$, NS: not significant; compared to the control-ASO group by one-way ANOVA with Dunnett correction for multiple comparisons. **g,h**, Effect of ASO treatment on the growth of MDA-PCa-2b xenografts in male athymic nude mice, with control ASO ($n = 15$) or *ARLNC1* ASO ($n = 13$) treatment subcutaneously at 50 mg per kg body weight, five times per week for 3 weeks. Tumors were measured by caliper biweekly (**g**) and tumor weights were measured at the end point (**h**). Mean ± s.d. values are shown. *$P = 0.0251$, ***$P < 0.0001$; compared to control ASO by two-tailed Student's t test. **i**, A model depicting the positive feedback loop between ARLNC1 and AR that is critical for prostate cancer growth.

Methods

References

1. Mercer, T. R., Dinger, M. E. & Mattick, J. S. Long non-coding RNAs: insights into functions. *Nat. Rev. Genet.* **10**, 155–159 (2009).
2. Wang, K. C. & Chang, H. Y. Molecular mechanisms of long noncoding RNAs. *Mol. Cell* **43**, 904–914 (2011).
3. Rinn, J. L. & Chang, H. Y. Genome regulation by long noncoding RNAs. *Annu. Rev. Biochem.* **81**, 145–166 (2012).
4. Rinn, J. L. et al. Functional demarcation of active and silent chromatin domains in human HOX loci by noncoding RNAs. *Cell* **129**, 1311–1323 (2007).
5. Lee, N., Moss, W. N., Yario, T. A. & Steitz, J. A. EBV noncoding RNA binds nascent RNA to drive host PAX5 to viral DNA. *Cell* **160**, 607–618 (2015).
6. Wutz, A., Rasmussen, T. P. & Jaenisch, R. Chromosomal silencing and localization are mediated by different domains of Xist RNA. *Nat. Genet.* **30**, 167–174 (2002).
7. Prensner, J. R. et al. The long noncoding RNA SChLAP1 promotes aggressive prostate cancer and antagonizes the SWI/SNF complex. *Nat. Genet.* **45**, 1392–1398 (2013).
8. Gupta, R. A. et al. Long non-coding RNA HOTAIR reprograms chromatin state to promote cancer metastasis. *Nature* **464**, 1071–1076 (2010).
9. Faghihi, M. A. et al. Expression of a noncoding RNA is elevated in Alzheimeras disease and drives rapid feed-forward regulation of β-secretase. *Nat. Med* **14**, 723–730 (2008).
10. Iyer, M. K. et al. The landscape of long noncoding RNAs in the human transcriptome. *Nat. Genet.* **47**, 199–208 (2015).
11. Malik, R. et al. The lncRNA PCAT29 inhibits oncogenic phenotypes in prostate cancer. *Mol. Cancer Res.* **12**, 1081–1087 (2014).
12. Shukla, S. et al. Identification and validation of PCAT14 as prognostic biomarker in prostate cancer. *Neoplasia* **18**, 489–499 (2016).
13. Lu-Yao, G. L. et al. Fifteen-year survival outcomes following primary androgen-deprivation therapy for localized prostate cancer. *JAMA Intern. Med.* **174**, 1460–1467 (2014).
14. Huggins, C. & Hodges, C. V. Studies on prostatic cancer. I. The effect of castration, of estrogen and of androgen injection on serum phosphatases in metastatic carcinoma of the prostate. 1941. *J. Urol.* **167**, 948–951 (2002).
15. The Veterans Administration Co-operative Urological Research Group. Treatment and survival of patients with cancer of the prostate. *Surg. Gynecol. Obstet.* **124**, 1011–1017 (1967).
16. Chen, Y., Sawyers, C. L. & Scher, H. I. Targeting the androgen receptor pathway in prostate cancer. *Curr. Opin. Pharmacol.* **8**, 440–448 (2008).
17. Wong, Y. N., Ferraldeschi, R., Attard, G. & de Bono, J. Evolution of androgen receptor targeted therapy for advanced prostate cancer. *Nat. Rev. Clin. Oncol.* **11**, 365–376 (2014).
18. Mukherji, D., Pezaro, C. J. & De-Bono, J. S. MDV3100 for the treatment of prostate cancer. *Expert Opin. Investig. Drugs* **21**, 227–233 (2012).
19. Scher, H. I. et al. Increased survival with enzalutamide in prostate cancer after chemotherapy. *N. Engl. J. Med.* **367**, 1187–1197 (2012).
20. Tran, C. et al. Development of a second-generation antiandrogen for treatment of advanced prostate cancer. *Science* **324**, 787–790 (2009).
21. Scher, H. I. et al. Antitumour activity of MDV3100 in castration-resistant prostate cancer: a phase 1-2 study. *Lancet* **375**, 1437–1446 (2010).
22. Stein, M. N., Goodin, S. & Dipaola, R. S. Abiraterone in prostate cancer: a new angle to an old problem. *Clin. Cancer Res.* **18**, 1848–1854 (2012).
23. Reid, A. H. et al. Significant and sustained antitumor activity in post-docetaxel, castration-resistant prostate cancer with the CYP17 inhibitor abiraterone acetate. *J. Clin. Oncol.* **28**, 1489–1495 (2010).
24. de Bono, J. S. et al. Abiraterone and increased survival in metastatic prostate cancer. *N. Engl. J. Med.* **364**, 1995–2005 (2011).
25. Watson, P. A., Arora, V. K. & Sawyers, C. L. Emerging mechanisms of resistance to androgen receptor inhibitors in prostate cancer. *Nat. Rev. Cancer* **15**, 701–711 (2015).
26. Antonarakis, E. S. et al. AR-V7 and resistance to enzalutamide and abiraterone in prostate cancer. *N. Engl. J. Med.* **371**, 1028–1038 (2014).
27. Attard, G., Richards, J. & de Bono, J. S. New strategies in metastatic prostate cancer: targeting the androgen receptor signaling pathway. *Clin. Cancer Res.* **17**, 1649–1657 (2011).
28. Hearn, J. W. et al. HSD3B1 and resistance to androgen-deprivation therapy in prostate cancer: a retrospective, multicohort study. *Lancet Oncol.* **17**, 1435–1444 (2016).
29. Chan, S. C., Li, Y. & Dehm, S. M. Androgen receptor splice variants activate androgen receptor target genes and support aberrant prostate cancer cell growth independent of canonical androgen receptor nuclear localization signal. *J. Biol. Chem.* **287**, 19736–19749 (2012).
30. Robinson, D. et al. Integrative clinical genomics of advanced prostate cancer. *Cell* **161**, 1215–1228 (2015).
31. Visakorpi, T. et al. In vivo amplification of the androgen receptor gene and progression of human prostate cancer. *Nat. Genet.* **9**, 401–406 (1995).
32. Asangani, I. A. et al. Therapeutic targeting of BET bromodomain proteins in castration-resistant prostate cancer. *Nature* **510**, 278–282 (2014).
33. Roche, P. J., Hoare, S. A. & Parker, M. G. A consensus DNA-binding site for the androgen receptor. *Mol. Endocrinol.* **6**, 2229–2235 (1992).
34. Pomerantz, M. M. et al. The androgen receptor cistrome is extensively reprogrammed in human prostate tumorigenesis. *Nat. Genet.* **47**, 1346–1351 (2015).
35. Cancer Genome Atlas Research Network. The molecular taxonomy of primary prostate cancer. *Cell* **163**, 1011–1025 (2015).
36. Takayama, K. et al. Androgen-responsive long noncoding RNA CTBP1-AS promotes prostate cancer. *EMBO J.* **32**, 1665–1680 (2013).
37. GTEx Consortium. The Genotype-Tissue Expression (GTEx) pilot analysis: multitissue gene regulation in humans. *Science* **348**, 648–660 (2015).
38. Mele, M. et al. The human transcriptome across tissues and individuals. *Science* **348**, 660–665 (2015).
39. Rhodes, D. R. et al. Oncomine 3.0: genes, pathways, and networks in a collection of 18,000 cancer gene expression profiles. *Neoplasia* **9**, 166–180 (2007).
40. Engreitz, J. M. et al. RNA-RNA interactions enable specific targeting of noncoding RNAs to nascent pre-mRNAs and chromatin sites. *Cell* **159**, 188–199 (2014).
41. Kretz, M. et al. Control of somatic tissue differentiation by the long non-coding RNA TINCR. *Nature* **493**, 231–235 (2013).
42. Gong, C. & Maquat, L. E. lncRNAs transactivate STAU1-mediated mRNA decay by duplexing with 3′ UTRs via Alu elements. *Nature* **470**, 284–288 (2011).
43. Gawronski, A. R. et al. MechRNA: prediction of lncRNA mechanisms from RNA-RNA and RNA-protein interactions. *Bioinformatics* (2018) https://doi.org/10.1093/bioinformatics/bty208
44. Mann, M., Wright, P. R. & Backofen, R. IntaRNA 2.0: enhanced and customizable prediction of RNA–RNA interactions. *Nucleic Acids Res.* **45**, W435–W439 (2017).
45. Lennox, K. A. & Behlke, M. A. Cellular localization of long non-coding RNAs affects silencing by RNAi more than by antisense oligonucleotides. *Nucleic Acids Res.* **44**, 863–877 (2016).
46. Meng, L. et al. Towards a therapy for Angelman syndrome by targeting a long non-coding RNA. *Nature* **518**, 409–412 (2015).
47. Wheeler, T. M. et al. Targeting nuclear RNA for in vivo correction of myotonic dystrophy. *Nature* **488**, 111–115 (2012).
48. Hua, Y. et al. Antisense correction of SMN2 splicing in the CNS rescues necrosis in a type III SMA mouse model. *Genes Dev.* **24**, 1634–1644 (2010).
49. Evers, M. M., Toonen, L. J. & van Roon-Mom, W. M. Antisense oligonucleotides in therapy for neurodegenerative disorders. *Adv. Drug Deliv. Rev.* **87**, 90–103 (2015).
50. Yeap, B. B. et al. Novel binding of HuR and poly(C)-binding protein to a conserved UC-rich motif within the 3'-untranslated region of the androgen receptor messenger RNA. *J. Biol. Chem.* **277**, 27183–27192 (2002).
51. Lebedeva, S. et al. Transcriptome-wide analysis of regulatory interactions of the RNA-binding protein HuR. *Mol. Cell* **43**, 340–352 (2011).

Author contributions

R. Malik, Y.Z., M.C., S.P. and A.M.C. conceived the study and designed the research. Y.Z. and R. Malik performed most of the cellular and molecular biology experiments with the assistance of Y.H., S.Y., S.S., S.K.S., L.X., X.J., S.M.D., X.C., J.T.W. and F.Y.F. M.C. performed most of the bioinformatics analyses with the help of Y.S.N. and M.K.I. S.P., U.P. and M.B. performed all smFISH work, and S.P. performed the mechanistic work-up. J.C.-Y.T. and K.M.J. carried out the in vivo mouse xenograft studies, and Y.Q. performed the 3D sphere model work. L.P.K. performed the histopathological analyses. L.W. and R. Mehra carried out RNA ISH on tissue microarrays, and T.-Y.L. and H.J. performed the statistical analysis for this technique. M.U., A.R.G., R.B. and C.S.S. performed the in silico binding predictions. S.M.F., A.T.W. and S.G. provided ASOs. G.C.S. provided the AR expression construct. M.T.P. and M.L. performed BrU and BrUChase sample preparation. Y.Z., M.C., R. Malik, S.P. and A.M.C. wrote the manuscript. All authors discussed the results and commented on the manuscript.

Competing interests

Additional information

Supplementary information is available for this paper at https://doi.org/10.1038/s41588-018-0120-1.

Reprints and permissions information is available at www.nature.com/reprints.

Correspondence and requests for materials should be addressed to A.M.C.

Publisher's note: Springer Nature remains neutral with regard to jurisdictional claims in published maps and institutional affiliations.

Methods

Cell lines. Cell lines were purchased from the American Type Culture Collection (ATCC) and maintained using standard media and conditions. All cell lines were genotyped by DNA fingerprinting analysis and tested for mycoplasma infection every 2 weeks. All cell lines used in this study were mycoplasma negative. For androgen stimulation experiments, VCaP and LNCaP cells were grown in medium supplemented with charcoal-stripped serum for 48 h and then stimulated with 10 nM DHT (Sigma-Aldrich) for 6 or 24 h.

RNA-seq. Total RNA was extracted from LNCaP and VCaP cells following DHT treatment, using the miRNeasy kit (Qiagen). RNA quality was assessed using an Agilent Bioanalyzer. Each sample was sequenced using the Illumina HiSeq 2000 (with a 100-nt read length) according to published protocols[52].

RNA-seq data analysis to identify AR-regulated genes. RNA-seq data were analyzed as previously described[53]. Briefly, the strand-specific paired-end reads were inspected for sequencing and data quality (for example, insert size, sequencing adaptor contamination, rRNA content, sequencing error rate). Libraries passing quality control were trimmed of sequencing adaptors and aligned to the human reference genome, GRCh38. Expression was quantified at the gene level using the 'intersection non-empty' mode[54] as implemented in featureCounts[55] using the Gencode v22[56] and/or MiTranscriptome[10] assemblies. All pairwise differential expression analyses were carried out using the voom–limma approach[57,58] with all default parameters. Relative expression levels (FPKM) were normalized for differences in sequencing depth using scaling factors obtained from the calcNormFactors (default parameters) function from edgeR[59].

ARGs were identified from expression data for VCaP and LNCaP cells treated with DHT for 6 and 24 h using three linear models: separate models for each of the cell lines treating the two time points as biological replicates and a merged model with all treated samples as replicates. ARGs were defined as genes that were significant (P value < 0.1 and absolute log fold change > 2) in both separate models and/or the merged model.

Identification of prostate cancer–associated protein-coding genes and lncRNAs. Raw RNA-seq data for patients with primary and metastatic prostate cancer were obtained from the TCGA/PRAD and PCF/SU2C projects, respectively. External transcriptome samples were reanalyzed using in-house pipelines (see above) to facilitate direct comparisons of expression levels and identification of differentially expressed genes. Pan-cancer analyses based on the MiTranscriptome assembly[10] were leveraged as FPKMs, and enrichment scores (SSEA) were computed as part of that project. Tissue lineage (prostate) and prostate cancer–specific genes were identified using the SSEA method as previously described[10]. Briefly, the SSEA test was used to determine whether each gene was significantly associated with a set of samples (for example, prostate cancer) or cancer progression in a given lineage (for example, prostate normal to prostate cancer). The genes were ranked according to their strength of association.

Oncomine concept analysis of the ARLNC1 signature. Genes with expression levels significantly correlated with ARLNC1 were separated into positively and negatively correlated gene lists. These two lists were then imported into Oncomine as custom concepts and queried for association with other prostate cancer concepts housed in Oncomine. All of the prostate cancer concepts with odds ratio > 2.0 and P value < 1 × 10^{-4} were selected. Top concepts (based on odds ratios) were selected for representation. We exported these results as the nodes and edges of a concept association network and visualized the network using Cytoscape version 3.3.0. Node positions were computed using the edge-weighted force-directed layout in Cytoscape using the odds ratio as the edge weight. Node positions were subtly altered manually to enable better visualization of Mode labels[60].

ChIP–seq data analysis. ChIP–seq data from published external and in-house datasets, GSE56288 and GSE55064, were reanalyzed using a standard pipeline. Briefly, groomed reads (vendor quality control, adaptor removal) were aligned to the GRCh38 reference genome using STAR settings that disable spliced alignment: outFilterMismatchNoverLmax: 0.05, outFilterMatchNmin: 16, outFilterScoreMinOverLread: 0, outFilterMatchNminOverLread: 0, alignIntronMax: 1. Improperly paired alignments and non-primary alignments were discarded. Peaks were called using MACS2 (callpeak --broad --qvalue 0.05 --broad-cutoff 0.05 and callpeak --call-summits --qvalue 0.05)[61] and Q (-n 100000)[62]. ChIP enrichment plots were computed from alignment coverage files (BigWig[63]) as trimmed (trim = 0.05) smooth splines (spar = 0.05). The baseline (non-specific) ChIP signal was estimated from genomic windows furthest from the center of the queried region (peak summit, TSS) and subtracted from each signal before plotting.

AR binding motif search. An unsupervised motif search was carried out using MEME[64]. DNA sequences (GRCh38) from the uni-peak ChIP–seq regions overlapping promoters (5 kb upstream, 1 kb downstream of the assembled or known TSS) of ARGs were used as input to MEME (default parameters).

ChIP–qPCR assays. AR, FOXA1 or NKX3-1 ChIP was performed following our previous protocol[32]. (Antibodies: AR, Millipore cat. no. 06-680; FOXA1, Thermo Fisher cat. no. PA5-27157; NKX3-1, CST cat. no. 83700S.) qPCR analysis was performed using the primers listed in Supplementary Table 3. Primers targeting the CYP2B7 promoter were purchased from CST (cat. no. 84846).

RNA ISH on tissue microarray. ISH assays were performed on tissue microarray sections from Advanced Cell Diagnostics as described previously[7]. In total, 133 tissue samples were included (11 from benign prostate, 85 from localized prostate cancer and 37 from metastatic prostate cancer). ARLNC1 ISH signals were examined in morphologically intact cells and scored manually by a study pathologist, using a previously described expression value scoring system[65]. For each tissue sample, the ARLNC1 product score was averaged across evaluable tissue microarray cores. Mean ARLNC1 product scores are plotted in Fig. 2e.

RACE. 5′ and 3′ RACE were performed to determine the transcriptional start and termination sites of ARLNC1, using the GeneRacer RLM-RACE kit (Invitrogen), according to the manufacturer's instructions.

Northern blot analysis. The NorthernMax-Gly Kit (Ambion) was used for ARLNC1 detection following the manufacturer's protocol. Briefly, 20 μg of total RNA was resolved on a 1% agarose glyoxal gel and then transferred to nylon membrane (Roche), cross-linked to the membrane (UV Stratalinker 1800; Stratagene) and the membrane was prehybridized. Overnight hybridization was performed with an ARLNC1-specific ^{32}P-labeled RNA probe. Membranes were exposed to HyBlot CL autoradiography film (Denville Scientific). The primer sequences used for generating the probes are given in Supplementary Table 3.

RNA isolation and cDNA synthesis. Total RNA from cell lines was isolated using QIAzol Lysis reagent (Qiagen) and the miRNeasy kit (Qiagen) with DNase digestion according to the manufacturer's instructions. cDNA was synthesized using Superscript III (Invitrogen) and random primers (Invitrogen).

qRT–PCR analysis. Relative RNA levels determined by qRT–PCR were measured on an Applied Biosystems 7900HT Real-Time PCR System, using Power SYBR Green MasterMix (Applied Biosystems). All primers were obtained from Integrated DNA Technologies, and gene-specific sequences are listed in Supplementary Table 3. GAPDH, HMBS or ACTB was used as an internal control for quantification of gene targets. The relative expression of RNAs was calculated using the ΔΔCt method.

Cytoplasmic and nuclear RNA purification. Cell fractionation was performed using the NE-PER nuclear extraction kit (Thermo Scientific) according to the manufacturer's instructions. RNA was extracted using the previously mentioned protocol.

siRNA-mediated knockdown. siRNA oligonucleotides targeting ARLNC1, AR, FOXA1, BRD4, NKX3-1, LSD1, IRF1, POU1F1 or EZH2 and a non-targeting siRNA were purchased from Dharmacon. (si-AR-pool, cat. no. L-003400-00-0005; si-FOXA1, cat. no. LU-010319-00-0005; si-BRD4, cat. no. LU-004937-00-0002; si-NKX3-1, cat. no. LU-015422-00-0005; si-LSD1, cat. no. LU-009223-00-0002; si-IRF1, cat. no. LU-011704-00-0005; si-POU1F1, cat. no. LU-012546-00-0005; si-EZH2, cat. no. L-004218-00-0005; si-NT, cat. no. D-001810-01-05.) siRNA sequences for ARLNC1 knockdown are listed in Supplementary Table 3. For AR knockdown, two more siRNAs were purchased from Life Technologies (no. HSS179972 and no. HSS179973). Transfections with siRNA (50 nM) were performed with Lipofectamine RNAiMAX according to the manufacturer's instructions. RNA and protein were harvested for analysis 72 h after transfection.

ASO-mediated knockdown. ASOs targeting ARLNC1 were obtained from Ionis Pharmaceuticals. Transfections with ASOs (50 nM) were performed with Lipofectamine RNAiMAX according to the manufacturer's instructions. RNA and protein were harvested for analysis 72 h after transfection.

Gene expression profiling. Total RNA was extracted following the aforementioned protocol. RNA integrity was assessed using an Agilent Bioanalyzer. Microarray analysis was carried out on the Agilent Whole Human Oligo Microarray platform, according to the manufacturer's protocol. siRNA-mediated knockdown experiments were run in triplicate, comparing knockdown samples treated with two independent ARLNC1 siRNAs to samples treated with non-targeting control siRNA. ASO-mediated knockdown experiments were run in replicate, comparing knockdown samples treated with two ARLNC1 ASOs to samples treated with non-targeting control. An AR signature was generated using MDA-PCa-2b cells treated with 10 nM DHT in triplicate.

Analysis of Agilent 44k microarrays was carried out using limma and included background subtraction (bc.method = 'half', offset = 100) and within-array normalization (method = 'loess'). Between-array quantile normalization of average expression levels (but not log-transformed fold change) was performed using the function normalizeBetweenArrays (method = 'Aquantile'). Control probes and

probes with missing values were excluded from further analyses. Probes were annotated to Gencode v22 genes using the mapping downloaded from Ensembl (efg_agilent_wholegenome_4×44k_v2). Probes originally annotated as AK093002 were used to detect ARLNC1. Differentially expressed genes following *ARLNC1* knockdown in MDA-PCA-2b cells were identified from triplicate biological repeats using adjusted *P* value < 0.1 and absolute log fold change > 0.6 cutoffs. Consensus targets of *ARLNC1* knockdown using siRNA and ASOs were identified using a merged linear model (all ten samples treated as replicates) and a *P* value < 0.001 cutoff.

GSEA. Enrichment analyses for custom and experimentally derived signatures (that is, AR targets, genes upregulated and downregulated following DHT treatment) were carried out using the non-parametric GSEA software with all default settings. For GO term enrichment, we applied the parametric randomSet[66] enrichment statistic to voom–limma-estimated fold changes (see above).

Overexpression of ARLNC1. Full-length ARLNC1 was amplified from MDA-PCa-2b cells and cloned into the pCDH clone and expression vector (System Biosciences). Insert sequences were validated by Sanger sequencing at the University of Michigan Sequencing Core. The full-length sequence for ARLNC1 expression is listed in Supplementary Table 4.

smFISH. smFISH and image analysis were performed as described previously[67,68]. Probe sequences targeting ARLNC1, PCAT1, DANCR, *AR*, *EZH2* and *FOXA1* were designed using the probe design software at https://www.biosearchtech.com/stellaris-designer and are listed in Supplementary Table 5. TERRA probes were designed as described previously[69]. Other probes were purchased directly from LGC-Biosearch. U2OS cells were seeded in six-well dishes and transfected with ARLNC1-expression vector alone or in combination with AR expression vector, using Fugene-HD (Promega) according to the manufacturer's protocol. Cells were incubated for 24 h, reseeded into eight-well chambered coverglasses, and fixed in formaldehyde for smFISH (as described above) after 24 h.

RNA in vitro transcription. Linearized DNA templates for full-length ARLNC1, ARLNC1 fragments, ARLNC1 deletion, antisense ARLNC1, LacZ, SChLAP1-AS, THOR and AR-3′ UTR-1–980 were synthesized using T7-containing primers. In vitro transcription assays were performed with T7 RNA polymerase (Promega) according to the manufacturer's instructions. For BrU-labeled RNA synthesis, 5-bromo-UTP was added to the transcription mix. At the end of transcription, DNA templates were removed by Turbo DNase (Thermo Fisher), and RNA was recovered using the RNA Clean and Concentrator Kit (Promega). RNA size and quality were further confirmed by Agilent Bioanalyzer.

RNA–RNA in vitro interaction assays. Twenty-five microlitres of Protein A/G Magnetic Beads (Pierce) was washed twice with RIP wash buffer (Millipore, cat. no. CS203177) before incubating with BrU antibody for 1 h at room temperature. After antibody conjugation, beads were washed twice with RIP wash buffer and then resuspended in incubation buffer containing RIP wash buffer, 17.5 mM EDTA (Millipore, cat. no. CS203175) and RNase Inhibitor (Millipore, cat. no. CS203219). Equal amounts (5 pmol) of BrU-labeled RNAs (ARLNC1, ARLNC1-AS, ARLNC1-1–1300, ARLNC1-1301–2786, ARLNC1-1–700, ARLNC1-701–1300, ARLNC1-del-701–1300, *LacZ*, SChLAP1-AS, THOR) were incubated with beads in Incubation Buffer for 2 h at 4 °C. Following incubation, 2.5 pmol of the *AR* 3′ UTR-1–980 RNA fragment was added into individual tubes and incubated overnight at 4 °C. After incubation, beads were washed six times with RIP Wash Buffer. To recover RNA, beads were digested with proteinase K buffer containing RIP Wash Buffer, 1% SDS (Millipore, cat. no. CS203174) and 1.2 μg/μl proteinase K (Millipore, cat. no. CS203218) at 55 °C for 30 min with shaking. After digestion, RNA was extracted from supernatant using the miRNeasy kit (Qiagen), and reverse transcription was performed using the Superscript III system (Invitrogen). The amount of *AR* 3′ UTR-1–980 recovered in each interaction assay was quantified by qPCR analysis. Data were normalized to the ARLNC1-AS control, using the ΔCt method. We designed ASOs blocking the *AR*–ARLNC1 interaction site (ASO-blocking, Ionis Pharmaceuticals) and used them in the in vitro interaction assays. Data were normalized to the control ASO, using the ΔCt method.

RNA stability assays. LNCaP cells were treated with 5 μg/ml actinomycin D for various times as indicated. RNA was extracted and qRT–PCR was carried out as described above. RNA half-life ($t_{1/2}$) was calculated by linear regression analysis.

Cell proliferation assays. Cells treated with siRNAs or ASOs were seeded into 24-well plates and allowed to attach. Cell proliferation was recorded by IncuCyte live-cell imaging system (Essen Biosciences), following the manufacturer's instructions.

Apoptosis analysis. Cells were grown in six-well plates and transfected with nonspecific siRNA or siRNAs targeting *ARLNC1*. Apoptosis analysis was performed 48 h after transfection, using the Dead Cell Apoptosis Kit (Molecular Probes no. V13241) according to the manufacturer's instructions.

Immunoblot analysis. Cells were lysed in RIPA lysis and extraction buffer (Thermo Scientific no. 89900) supplemented with protease inhibitor cocktail (Roche no. 11836170001). Protein concentrations were quantified using the DC protein assay (Bio-Rad), and protein lysates were boiled in sample buffer. Protein extracts were then loaded and separated on SDS–PAGE gels. Blotting analysis was performed with standard protocols using polyvinylidene difluoride membrane (GE Healthcare). Membranes were blocked for 60 min in blocking buffer (5% milk in a solution of 0.1% Tween-20 in Tris-buffered saline (TBS-T)) and then incubated overnight at 4 °C with primary antibody. After three washes with TBS-T, membranes were incubated with horseradish peroxidase (HRP)-conjugated secondary antibody. Signals were visualized with an enhanced chemiluminescence system as described by the manufacturer (Thermo Scientific Pierce ECL Western Blotting Substrate). Primary antibodies used were as follows: androgen receptor (1:1,000 dilution, Millipore, no. 06-680, rabbit), GAPDH (1:5,000 dilution, Cell Signaling, no. 3683, rabbit), PSA (KLK3) (1:5,000 dilution, Dako, no. A0562, rabbit) and cleaved PARP (1:1,000 dilution, Cell Signaling, no. 9542, rabbit).

Androgen receptor reporter gene assays. Dual-luciferase reporter assays were performed using the Cignal Androgen Receptor Reporter Kit (Qiagen) according to the manufacturer's instructions. Briefly, cells were cotransfected with siRNAs (nonspecific, targeting *AR* or *ARLNC1*) and reporter vectors (negative control or AR reporter), using Lipofectamine 2000 transfection reagent (Thermo Fisher Scientific). Forty hours after transfection, DHT (or ethanol vehicle control) was added to induce AR signaling. The Dual-Luciferase assay was conducted 8 h after DHT stimulation, using the Dual-Luciferase Reporter Assay System from Promega (cat no. 1910). Reporter activity was analyzed on the basis of the ratio of firefly/*Renilla* activity to normalize for cell number and transfection efficiency.

In vivo experiments. All experiments were approved by the University of Michigan Institutional Animal Care and Use Committee. For tumor generation with shRNA-mediated knockdown, shRNA targeting *ARLNC1* was cloned into pSIH1-H1-copGFP-T2A-Puro (System Biosciences). Lentiviral particles were generated at the University of Michigan Vector Core. LNCaP-AR cells were infected with lentivirus expressing *ARLNC1* shRNA for 48 h. Knockdown of ARLNC1 was confirmed by qPCR analysis. Male athymic nude mice were randomized into two groups at 6 to 8 weeks of age. Five million cells expressing sh-*ARLNC1* or sh-vector were injected into bilateral flanks of mice. Caliper measurements were taken in two dimensions twice a week by an investigator blinded to the study objective and used to calculate tumor volume. The study was terminated when the tumor volume reached 1,000 mm³. For ASO treatment in vivo, 6- to 8-week-old male athymic nude mice were inoculated subcutaneously with MDA-PCa-2b cells suspended in a Matrigel scaffold in the posterior dorsal flank region (5 million cells per site, two sites per animal). When the mean tumor volume reached approximately 150 mm³, mice were randomized into two groups and treated with *ARLNC1*-specific or control ASO. ASOs, dosed at 50 mg per kg body weight, were subcutaneously injected between the scapulae once daily for three periods of 5 d on/2 d off. Tumor size was measured twice per week using a digital caliper by a researcher blinded to the study design. Mouse body weights were monitored throughout the dosing period. When the average tumor size in the control group reached 1,500 mm³, mice were euthanized and the primary tumors were excised for weight determination. One-third of the resected specimen was placed in 10% formalin buffer, and the remaining tissue was snap-frozen.

BrU-seq and BrUChase-seq. BrU-seq and BrUChase-seq assays were performed as previously described[70,71] with MDA-PCa-2b cells treated with either si-NT or si-*ARLNC1*. BrU labeling was performed for 30 min, and chase experiments were performed for 6 h.

Statistical analysis. For in vivo experiments, power analysis (GPOWER software) performed for each tumor type tested to date indicates that the sample size we chose yields a statistical power >90% for detection of tumor size reduction of 40%. Sample sizes were not predetermined for all other assays. For in vivo experiments, animals were randomized. Randomization was not performed for all other assays. Statistical analyses were performed using GraphPad Prism software or using R. Data are presented as either means ± s.e.m. or means ± s.d. All of the experiments were performed in biological triplicate unless otherwise specified. Statistical analyses shown in figures represent two-tailed *t* tests, one-way ANOVA, two-way ANOVA or Kruskal–Wallis rank-sum tests as indicated. $P < 0.05$ was considered to be statistically significant. Details regarding the statistical methods employed during microarray, RNA-seq and ChIP–seq data analysis were included in the aforementioned methods for bioinformatics analyses.

Reporting Summary. Further information on experimental design is available in the Nature Research Reporting Summary linked to this article.

Code availability. Software for transcriptome meta-assembly and lncRNA discovery is available at https://tacorna.github.io/.

Data availability. RNA-seq and microarray data sets generated from this study have been deposited into the Gene Expression Omnibus, with accession GSE110905. Other data supporting the findings of this study are included in the Supplementary Information.

References

52. Prensner, J. R. et al. Transcriptome sequencing across a prostate cancer cohort identifies PCAT-1, an unannotated lincRNA implicated in disease progression. *Nat. Biotechnol.* **29**, 742–749 (2011).
53. Cieslik, M. et al. The use of exome capture RNA-seq for highly degraded RNA with application to clinical cancer sequencing. *Genome Res.* **25**, 1372–1381 (2015).
54. Anders, S., Pyl, P. T. & Huber, W. HTSeq-a Python framework to work with high-throughput sequencing data. *Bioinformatics* **31**, 166–169 (2015).
55. Liao, Y., Smyth, G. K. & Shi, W. featureCounts: an efficient general purpose program for assigning sequence reads to genomic features. *Bioinformatics* **30**, 923–930 (2014).
56. Harrow, J. et al. GENCODE: the reference human genome annotation for The ENCODE Project. *Genome Res.* **22**, 1760–1774 (2012).
57. Law, C. W., Chen, Y., Shi, W. & Smyth, G. K. voom: precision weights unlock linear model analysis tools for RNA-seq read counts. *Genome Biol.* **15**, R29 (2014).
58. Ritchie, M. E. et al. limma powers differential expression analyses for RNA-sequencing and microarray studies. *Nucleic Acids Res.* **43**, e47 (2015).
59. Robinson, M. D., McCarthy, D. J. & Smyth, G. K. edgeR: a Bioconductor package for differential expression analysis of digital gene expression data. *Bioinformatics* **26**, 139–140 (2010).
60. Cline, M. S. et al. Integration of biological networks and gene expression data using Cytoscape. *Nat. Protoc.* **2**, 2366–2382 (2007).
61. Zhang, Y. et al. Model-based analysis of ChIP-Seq (MACS). *Genome Biol.* **9**, R137 (2008).
62. Hansen, P. et al. Saturation analysis of ChIP-seq data for reproducible identification of binding peaks. *Genome Res.* **25**, 1391–1400 (2015).
63. Kent, W. J., Zweig, A. S., Barber, G., Hinrichs, A. S. & Karolchik, D. BigWig and BigBed: enabling browsing of large distributed datasets. *Bioinformatics* **26**, 2204–2207 (2010).
64. Bailey, T. L. et al. MEME SUITE: tools for motif discovery and searching. *Nucleic Acids Res.* **37**, W202–W208 (2009).
65. Mehra, R. et al. A novel RNA in situ hybridization assay for the long noncoding RNA SChLAP1 predicts poor clinical outcome after radical prostatectomy in clinically localized prostate cancer. *Neoplasia* **16**, 1121–1127 (2014).
66. Newton, M. A., Quintana, F. A., Den Boon, J. A., Sengupta, S. & Ahlquist, P. Random-set methods identify distinct aspects of the enrichment signal in gene-set analysis. *Ann. Appl. Stat.* **1**, 85–106 (2007).
67. Raj, A., van den Bogaard, P., Rifkin, S. A., van Oudenaarden, A. & Tyagi, S. Imaging individual mRNA molecules using multiple singly labeled probes. *Nat. Methods* **5**, 877–879 (2008).
68. Niknafs, Y. S. et al. The lncRNA landscape of breast cancer reveals a role for DSCAM-AS1 in breast cancer progression. *Nat. Commun.* **7**, 12791 (2016).
69. Rossiello, F. et al. DNA damage response inhibition at dysfunctional telomeres by modulation of telomeric DNA damage response RNAs. *Nat. Commun.* **8**, 13980 (2017).
70. Paulsen, M. T. et al. Coordinated regulation of synthesis and stability of RNA during the acute TNF-induced proinflammatory response. *Proc. Natl Acad. Sci. USA* **110**, 2240–2245 (2013).
71. Paulsen, M. T. et al. Use of Bru-Seq and BruChase-Seq for genome-wide assessment of the synthesis and stability of RNA. *Methods* **67**, 45–54 (2014).

natureresearch

Corresponding author(s):   Arul M. Chinnaiyan

Reporting Summary

Nature Research wishes to improve the reproducibility of the work that we publish. This form provides structure for consistency and transparency in reporting. For further information on Nature Research policies, see Authors & Referees and the Editorial Policy Checklist.

Statistical parameters

When statistical analyses are reported, confirm that the following items are present in the relevant location (e.g. figure legend, table legend, main text, or Methods section).

n/a	Confirmed	
☐	☒	The exact sample size (*n*) for each experimental group/condition, given as a discrete number and unit of measurement
☐	☒	An indication of whether measurements were taken from distinct samples or whether the same sample was measured repeatedly
☐	☒	The statistical test(s) used AND whether they are one- or two-sided *Only common tests should be described solely by name; describe more complex techniques in the Methods section.*
☐	☒	A description of all covariates tested
☐	☒	A description of any assumptions or corrections, such as tests of normality and adjustment for multiple comparisons
☐	☒	A full description of the statistics including central tendency (e.g. means) or other basic estimates (e.g. regression coefficient) AND variation (e.g. standard deviation) or associated estimates of uncertainty (e.g. confidence intervals)
☐	☒	For null hypothesis testing, the test statistic (e.g. F, t, r) with confidence intervals, effect sizes, degrees of freedom and P value noted *Give P values as exact values whenever suitable.*
☒	☐	For Bayesian analysis, information on the choice of priors and Markov chain Monte Carlo settings
☒	☐	For hierarchical and complex designs, identification of the appropriate level for tests and full reporting of outcomes
☐	☒	Estimates of effect sizes (e.g. Cohen's *d*, Pearson's *r*), indicating how they were calculated
☐	☒	Clearly defined error bars *State explicitly what error bars represent (e.g. SD, SE, CI)*

Our web collection on statistics for biologists may be useful.

Software and code

Policy information about availability of computer code

Data collection	RNA seq, Microarray and qRT-PCR data were collected using vendor's software on Illumina HiSeq 2000, Agilent Whole Human Oligo Microarray, Applied Biosystems 7900HT Real-Time PCR platforms respectively. Microscopy images were acquired using Metamorph.
Data analysis	Software for transcriptome meta-assembly and lncRNAs discovery is available at https://tacorna.github.io/. Gene signatures were obtained using GSEA software. Image analysis was performed using custom-written macros in Image J and can be shared upon request. Statistical analysis was performed using Graphpad-Prism 6.0 and R.

For manuscripts utilizing custom algorithms or software that are central to the research but not yet described in published literature, software must be made available to editors/reviewers upon request. We strongly encourage code deposition in a community repository (e.g. GitHub). See the Nature Research guidelines for submitting code & software for further information.

Data

Policy information about availability of data

All manuscripts must include a data availability statement. This statement should provide the following information, where applicable:

- Accession codes, unique identifiers, or web links for publicly available datasets
- A list of figures that have associated raw data
- A description of any restrictions on data availability

RNA-seq and microarray datasets generated from this study have been deposited into Gene Expression Omnibus, with accession number: GSE110905. Other data supporting the finding of this study are included in the Supplementary Information files. Software for transcriptome meta-assembly and lncRNAs discovery is available at https://tacorna.github.io/. We have no restrictions on data availability and data can be shared upon request.

Field-specific reporting

Please select the best fit for your research. If you are not sure, read the appropriate sections before making your selection.

☒ Life sciences   ☐ Behavioural & social sciences

For a reference copy of the document with all sections, see nature.com/authors/policies/ReportingSummary-flat.pdf

Life sciences

Study design

All studies must disclose on these points even when the disclosure is negative.

Sample size	For in vivo experiments, power analysis (GPOWER software) performed for each tumor type tested to date indicates this animal number yields a statistical power >90% for detection of tumor size reduction of 40%. Sample sizes were not pre-determined for all other assays.
Data exclusions	No data were excluded.
Replication	All experiments were carried out at least 3 independent times for statistical reproducibility, unless otherwise stated, as represented by p-values.
Randomization	For in vivo experiments, animals were randomized. Randomization was not performed for all other assays.
Blinding	For in vivo experiments, tumor size was measured twice per week using a digital caliper by a researcher blinded to the study design. Blinding was not performed for all other assays.

Materials & experimental systems

Policy information about availability of materials

n/a	Involved in the study
☒	☐ Unique materials
☐	☒ Antibodies
☐	☒ Eukaryotic cell lines
☐	☒ Research animals
☒	☐ Human research participants

Antibodies

Antibodies used	Primary antibodies used in this study were: Androgen Receptor (1:1000 dilution, Millipore, #06-680, rabbit), GAPDH (1:5000 dilution, Cell Signaling, #3683, rabbit), PSA (1:5000 dilution, Dako, #A0562, rabbit), FOXA1 (Thermo Fisher Cat# PA5-27157) NKX3.1 (CST Cat# 83700S) and cleaved PARP (1:1000 dilution, Cell Signaling, #9542, rabbit).
Validation	All antibodies were validated by the vendors. Androgen receptor and PSA antibodies were also validated by siRNA treatment and androgen signaling assays respectively.

Eukaryotic cell lines

Policy information about cell lines

Cell line source(s)	All cell lines were purchased form ATCC.
Authentication	All cell lines were genotyped by STR profiling in house based on ATCC markers.

Mycoplasma contamination	All cells were tested for mycoplasma every two weeks.
Commonly misidentified lines (See ICLAC register)	Study does not include misidentified lines.

Research animals

Policy information about studies involving animals; ARRIVE guidelines recommended for reporting animal research

Animals/animal-derived materials	Male athymic nude mice were used in our in vivo studies.

Method-specific reporting

n/a	Involved in the study
☒ ☐	ChIP-seq
☒ ☐	Flow cytometry
☒ ☐	Magnetic resonance imaging